

# **CSP-free adaptive Kriging surrogate model method for reliability analysis with small failure probability**

Wenxiong Li\*, Rong Geng, Suiyin Chen

College of Water Conservancy and Civil Engineering, South China Agricultural University, Guangzhou

510642, China

\*Corresponding author. E-mail: leewenxiong@scau.edu.cn

**Abstract** In the field of reliability engineering, the Active learning reliability method combining Kriging and Monte Carlo Simulation (AK-MCS) has been developed and demonstrated to be effective in reliability analysis. However, the performance of AK-MCS is sensitive to the size of Candidate Sample Pool (CSP), particularly for systems with small failure probabilities. To address the limitations of conventional AK-MCS that relies on CSP, this paper proposes a CSP-free AK-MCS. The proposed methodology consists of two stages: surrogate model construction and Monte Carlo simulation for estimating the failure probability. In the stage of surrogate model construction, the surrogate model is iteratively refined based on the representative samples selected by solving the optimization problem facilitated by Particle Swarm Optimization (PSO) algorithm. To achieve an optimal balance between solution accuracy and efficiency, the penalty intensity control and the density control for the experimental design points are introduced to modify the objective function in optimization. The performance of the proposed methodology is evaluated using numerical examples, and results indicate that by leveraging an optimization algorithm to select representative samples, the proposed CSP-free AK-MCS overcomes the limitations of conventional CSP-based AK-MCS and exhibits exceptional performance in addressing small failure probabilities.

**Keywords** Reliability analysis; Kriging surrogate model; Particle swarm optimization algorithm; Learning function; Candidate sample pool

## **1. Introduction**

Engineering systems are subject to a multitude of uncertain factors that can significantly impact their reliability and safety. The presence of uncertainties exposes the engineering system to the risk of failure, potentially resulting in severe consequences, including loss of life and property. Consequently, reliability analysis has garnered considerable attention in diverse engineering

domains such as mechanical systems, infrastructure engineering, automotive, and industrial robotics.

Over the past several decades, a plethora of reliability methodologies have been proposed. The First Order Reliability Method (FORM) and the Second Order Reliability Method (SORM) represent classical approaches to conducting system reliability analysis. These methodologies entail first-order and second-order Taylor expansions of the performance function, with the Most Probable Points (MPP) and value of the reliability index determined iteratively. However, due to the omission of high-order terms in the expansion, the solution precision of FORM and SORM is relatively low, rendering them unsuitable for addressing problems with highly nonlinear performance functions. Monte Carlo Simulation (MCS) [1] can be employed to ascertain the failure probability of components or systems through random simulation and statistical testing. This methodology is applicable for addressing a wide range of reliability problems with highly nonlinear and complex performance functions. Nevertheless, crude Monte Carlo simulation typically necessitates a large number of random samples and numerical simulations (such as finite element analysis) to determine the value of the performance function for each sample. This results in a significant time cost for reliability analysis. Consequently, crude Monte Carlo simulation is often utilized as a benchmark to gauge the merits and demerits of other methodologies but is challenging to directly apply to engineering works. In recent years, surrogate model methodologies have emerged as a novel solution scheme for system reliability analysis. These methodologies generally involve two steps: first, constructing a surrogate model to approximate the performance function based on Design of Experiment (DoE) data, which encompasses sample points for system uncertainties and corresponding performance function values; second, performing Monte Carlo simulation using the established surrogate model in lieu of the real performance function to calculate the system's failure probability. Unlike crude MCS, surrogate model methodologies can achieve significantly higher efficiency as repeated numerical simulations are required only for the samples in DoE, rather than all samples in MCS. Commonly employed surrogate models include polynomial response surface models [2], radial basis function models [3], Kriging models [4], neural network models [5], support vector machine models [6], and their combination models. The accuracy of the surrogate model is intimately linked to DoE data. Generally, representative samples are conducive to establishing high-precision surrogate models. In other words, when equivalent levels of accuracy are required, the scale of DoE for constructing the surrogate model can be reduced by utilizing representative samples. Conventional approaches to generating DoE data based on random sampling often fail to select representative sample points and it can be challenging to determine the

appropriate scale of DoE. As a result, the applicability of surrogate model methodologies is impacted. To address these challenges, adaptive surrogate model methodologies developed in recent years have provided a novel solution for reliability analysis.

The primary distinction between adaptive surrogate model methodologies and conventional surrogate model methodologies resides in the selection of samples for DoE. In adaptive methodologies, the surrogate model is established through incremental refinement, with a learning function typically employed to guide the selection of representative samples during model construction. In recent years, scholars have extensively debated the implementation and performance of adaptive methodologies based on various surrogate models, including support vector machine models [7, 8], radial basis function models [9], neural network models [10, 11], and Kriging models [12, 13]. Due to its precise interpolation and effective estimation of uncertainty, the Kriging model is commonly utilized to establish adaptive surrogate model methodologies. Echard et al. [14] proposed the AK-MCS for Active learning reliability method combining Kriging model and MCS. In this methodology, the U-learning function for a candidate point is determined based on the mean value and Kriging variance of its performance function. Faurat and Gayton [15] introduced the AK-SYS methodology by integrating AK-MCS with Efficient Global Reliability Analysis (EGRA) to analyze system reliability with multiple failure modes. Zhang et al. [16] employed the Reliability Expectation Improvement Function (REIF) to develop an active learning surrogate model methodology. Yun et al. [17] proposed an adaptive Kriging surrogate model methodology based on a modified U-learning function for system reliability analysis of problems with multiple failure modes. Xiao et al. [13] introduced an adaptive Kriging surrogate model methodology with a novel learning function based on cross-validation that accounts for both the epistemic uncertainty of surrogate models and the aleatory uncertainty of random variables. Xiao et al. [18] further explored the adaptive Kriging surrogate model methodology by considering multiple failure modes and mixed variables. Ma et al. [12] conducted a comparative study on the impact of initial DoE data, learning functions, and stopping criteria on the solution performance of an adaptive Kriging surrogate model methodology. Wang et al. [19] derived a quantificational error measure of Kriging models and presented the modified stepwise accuracy-improvement strategy to solve system reliability problems. Xiong and Sampath [20] proposed three methods including the candidate size control method, multiple trends method and weighted clustering method to improve algorithm performance of AK-MCS and give it the potential for parallel computing. Xiao et al. [21] proposed a learning function for selecting new training samples for complex systems and improved the computational efficiency of system reliability analysis by combining dependent Kriging predictions

and parallel learning strategy. Ma et al. [22] proposed a novel methodology for multiple limit-state functions within a single run including an adaptive Kriging-Monte Carlo simulation for multiple responses and an adaptive Kriging-generalized subset simulation.

Within the framework of AK-MCS, representative samples required for updating the surrogate model are typically obtained using a selection strategy based on the Candidate Sample Pool (CSP). It must be noted that the performance of AK-MCS is sensitive to the size of CSP. Especially, to estimate small failure probabilities, a large-scale CSP is necessary to obtain a robust and convergent failure probability estimate. During the process of updating the Kriging model, the AK-MCS methodology must estimate the learning function value for all samples in CSP to iteratively select new training samples. This process is time-consuming and reduces the efficiency of the AK-MCS methodology for estimating small failure probabilities. To enhance the efficiency of the AK-MCS methodology for estimating small failure probability, numerous improved AK-MCS methodologies have been proposed. Echard et al. [23] proposed the AK-IS methodology by combining AK-MCS with an importance sampling methodology. Balesdent et al. [24] and Zhao et al. [25] conducted research on the combination of an adaptive Kriging surrogate model and importance sampling methodology. Yun et al. [26] proposed the AK-MIS methodology that combines an adaptive Kriging surrogate model and modified importance sampling to further distinguish important regions from unimportant ones based on AK-IS, with a Kriging surrogate model constructed in the important regions. Sun et al. [27] presented an adaptive Kriging surrogate model methodology based on the Least Improved Function (LIF), which combines Markov Chain Monte Carlo simulation (MCMC) to address problems with nonlinear performance functions and small failure probabilities. Building on AK-MCS and K-weighted-means clustering, Lelièvre et al. [28] introduced multipoint enhancement technology and developed AK-MCSi for reliability analysis. Lv et al. [29] proposed a novel learning function based on information entropy for the Kriging methodology and introduced the AK-LS methodology, which combines active learning Kriging model with line sampling, to ensure the reliability of complex structures with small failure probability and multidimensional variables. Xiao et al. [13] developed an adaptive Kriging surrogate model methodology by introducing adaptive importance sampling. Zhou et al. [30] introduced an adaptive Kriging surrogate model methodology that employs a point selection strategy with a limited region, defined as the region that significantly contributes to the accuracy of the surrogate model. Xu et al. [31] proposed a modified algorithm that combines AK-MCS and modified subset simulation to estimate small failure probabilities. Yun et al. [32] presented an improved AK-MCS based on adaptive radial-based importance sampling used to reduce the number of candidate points in the AK-MCS

methodology. Liu et al. [33] developed an enhanced AK-MCS by utilizing an efficient CSP reduction strategy. Song et al. [34] proposed a failure boundary exploration and exploitation framework by combining the adaptive Kriging model and sample space partitioning strategy to improve the computational efficiency and avoid memory problems. Wang et al. [35] proposed a novel adaptive Kriging method by combining sampling region scheme and error-based stopping criterion for structural reliability analysis. The improvements to AK-MCS mentioned above generally aim to reduce the size of CSP while ensuring accurate and robust estimation of failure probability. These methods primarily achieve the reduction through advanced sampling techniques or important region selection, thereby improving the efficiency of constructing a Kriging model for the actual performance function. However, there are limitations to their application compared to direct MCS. For example, the MPP is required, which presents challenges for problems with multiple MPPs. Additionally, subset simulation used in AK-MCS requires generating conditional samples through Markov Chain Monte Carlo simulation and approximating the performance function corresponding to each intermediate failure event. The total number of model evaluations for these methods may be larger than that of the AK-MCS.

Considering the limitations of CSP-based AK-MCS methods, developing AK-MCS methods that do not rely on CSP is a growing trend. The selection of representative points in AK-MCS is fundamentally an optimization problem. In recent years, research on adaptive surrogate models based on optimization algorithms has made significant progress [9, 36-38]. Jing et al. [37] developed an adaptive surrogate model method using radial basis function, where the “potential” MPP for updating the surrogate model is obtained by solving a constrained optimization problem using the genetic algorithm. In their work, the distances between the identified “potential” MPP and the existing DoE are dynamically controlled by a distance constraint. Meng et al. [38] proposed an adaptive Kriging surrogate model method where the representative samples are selected using the Particle Swarm Optimization (PSO) algorithm [39, 40] with an active weight learning function. In their work, the learning function is constructed based on three factors: the predicted mean value and Kriging variance of the performance function, as well as the joint probability density function (PDF) of random variables. These achievements have advanced the development of surrogate model methods. These optimization-based adaptive surrogate model methods can be further improved by addressing the following issues. Firstly, it is necessary to predict the performance function values for all samples in the Monte Carlo population during the construction of surrogate model, because the stopping criteria is related to the estimated failure probability. For the problems with small failure probabilities, the size of the Monte Carlo population is large and predicting the performance

function values for this population is time-consuming, even when using a surrogate model. Another issue concerns the definition of the objective function for the optimization problem. Typically, a constrained optimization problem is transformed into an unconstrained optimization problem with a penalty term. Then, determining an appropriate penalty intensity becomes a new issue in defining the objective function. To the best of the authors' knowledge, it is challenging to achieve optimal results in different specific problems using an uniform penalty intensity.

To address the limitations of CSP-based adaptive Kriging surrogate model methods and existing optimization-based adaptive surrogate model methods, this paper proposes an improved AK-MCS for reliability analysis. In the proposed methodology, the surrogate model is iteratively refined based on the representative samples selected by solving the optimization problem facilitated by PSO, with the same stopping criteria as AK-MCS. As a result, the implementation of the proposed method is divided into two stages: surrogate model construction and MCS with the established surrogate model for estimating the failure probabilities. This approach avoids predicting the performance function values for all samples in the Monte Carlo population during surrogate model construction. Based on the U-learning function used in AK-MCS, the new objective function for the optimization problem is defined, incorporating penalty intensity control and density control for experimental design points. This allows for an optimal balance between solution accuracy and efficiency to be achieved. Finally, the performance of the proposed methodology is evaluated using numerical examples.

## 2. AK-MCS

This section introduces the regular CSP-based AK-MCS [12, 14, 15, 28]. Firstly, the specific form of the Kriging model used in AKMCS is presented. Then, the principles and implementation of AK-MCS for reliability analysis are introduced and discussed.

### 2.1. Kriging model

Kriging model is a nonlinear interpolation meta-model developed for geostatistics. In system reliability analysis, Kriging model can be used as a surrogate model to approximate the relationship between system input and output, such as the relationship between the sampling points and the performance function values corresponding to these sampling points. Generally, Kriging model consists of two parts, i.e. a parametric linear regression model and a nonparametric stochastic process. The approximate relationship between any experiment  $\mathbf{x} = (x_1, x_2, \dots, x_n)^T$  and the response  $\hat{G}(\mathbf{x})$  can be denoted as

$$\hat{G}(\mathbf{x}) = \mathbf{f}^T(\mathbf{x})\boldsymbol{\beta} + z(\mathbf{x}) \quad (1)$$

where  $\mathbf{f}^T(\mathbf{x})\boldsymbol{\beta}$  represents the deterministic part which gives an approximation of the response in mean,  $\mathbf{f}^T(\mathbf{x}) = \{f_1(\mathbf{x}), f_2(\mathbf{x}), \dots, f_k(\mathbf{x})\}$  represents the basis function vector and  $\boldsymbol{\beta}^T = \{\beta_1, \beta_2, \dots, \beta_k\}$  is the regression coefficient vector. In this paper, ordinary Kriging model is selected which means that  $f_i(\mathbf{x}) = 1$  ( $i = 1, 2, \dots, k$ ). In Eq.(1),  $z(\mathbf{x})$  is a stationary Gaussian process with zero mean  $z(\mathbf{x}) \sim N(0, \sigma^2)$ , and the covariance between two points of space  $\mathbf{x}^i$  and  $\mathbf{x}^j$  is defined as

$$\text{Cov}[z(\mathbf{x}^i), z(\mathbf{x}^j)] = \sigma^2 R(\boldsymbol{\theta}, \mathbf{x}^i, \mathbf{x}^j) \quad (2)$$

where  $\sigma^2$  is the process variance,  $\boldsymbol{\theta} = \{\theta_1, \theta_2, \dots, \theta_n\}$  refers to the parameter vector, and  $R(\boldsymbol{\theta}, \mathbf{x}^i, \mathbf{x}^j)$  represents the correlation function between  $\mathbf{x}^i$  and  $\mathbf{x}^j$ , which is formulated by

$$R(\boldsymbol{\theta}, \mathbf{x}^i, \mathbf{x}^j) = \prod_{d=1}^n \exp\left[-\theta_d (x_d^i - x_d^j)^2\right] \quad (3)$$

where  $x_d^i$  and  $x_d^j$  refers to the  $d^{\text{th}}$  component in  $\mathbf{x}^i$  and  $\mathbf{x}^j$ , respectively.

Given the sample set of DoE  $\mathbf{S}_{\text{DoE}} = [\mathbf{x}^1, \mathbf{x}^2, \dots, \mathbf{x}^m]$  and the corresponding response set  $\mathbf{Y}_{\text{DoE}} = [G(\mathbf{x}^1), G(\mathbf{x}^2), \dots, G(\mathbf{x}^m)]$  with  $m$  being the number of samples in DoE, the scalars  $\beta$  and  $\sigma^2$  are estimated by

$$\hat{\beta} = (\mathbf{1}^T \mathbf{R}^{-1} \mathbf{1})^{-1} \mathbf{R}^{-1} \mathbf{Y}_{\text{DoE}} \quad (4)$$

$$\hat{\sigma}^2 = \frac{1}{m} (\mathbf{Y}_{\text{DoE}} - \hat{\beta} \mathbf{1})^T \mathbf{R}^{-1} (\mathbf{Y}_{\text{DoE}} - \hat{\beta} \mathbf{1}) \quad (5)$$

where  $\mathbf{R}$  is the correlation matrix with the component  $R_{i,j} = R(\boldsymbol{\theta}, \mathbf{x}^i, \mathbf{x}^j)$  in which represents the correlation between each pair of points in DoE, and  $\mathbf{1}$  refers to the vector filled with 1 of length  $m$ .  $\hat{\beta}$  and  $\hat{\sigma}^2$  in Eqs. (4) and (5) are related to the correlation parameters  $\theta_i$  through the matrix  $\mathbf{R}$ , then the value of  $\boldsymbol{\theta}$  is required to be firstly obtained by using maximum likelihood estimation:

$$\boldsymbol{\theta} = \arg \min_{\boldsymbol{\theta}} (\det(\mathbf{R}))^{\frac{1}{m}} \hat{\sigma}^2 \quad (6)$$

According to the Gaussian process regression theory, the system response follows the normal distribution as  $G(\mathbf{x}) \sim N(\mu_G(\mathbf{x}), \sigma_G(\mathbf{x}))$ . Then, based on the Kriging model established according to the given data of DoE, the Best Linear Unbiased Predictor (BLUP) of the response  $\hat{G}(\mathbf{x})$  at an

unknown point  $\mathbf{x}$  is shown to be a Gaussian random variate  $\hat{G}(\mathbf{x}) \sim N(\mu_{\hat{G}}(\mathbf{x}), \sigma_{\hat{G}}(\mathbf{x}))$  where

$$\mu_{\hat{G}}(\mathbf{x}) = \hat{\beta} + \mathbf{r}(\mathbf{x}) \mathbf{R}^{-1} (\mathbf{Y}_{\text{DoE}} - \hat{\beta} \mathbf{1}) \quad (7)$$

$$\sigma_{\hat{G}}^2(\mathbf{x}) = \hat{\sigma}^2 \left( \mathbf{1} - \mathbf{r}^T(\mathbf{x}) \mathbf{R}^{-1} \mathbf{r}(\mathbf{x}) + \mathbf{u}^T(\mathbf{x}) (\mathbf{1}^T \mathbf{R}^{-1} \mathbf{1})^{-1} \mathbf{u}(\mathbf{x}) \right) \quad (8)$$

where  $\mathbf{r}(\mathbf{x}) = [R(\mathbf{0}, \mathbf{x}, \mathbf{x}^1), R(\mathbf{0}, \mathbf{x}, \mathbf{x}^2), \dots, R(\mathbf{0}, \mathbf{x}, \mathbf{x}^m)]^T$  and  $\mathbf{u}(\mathbf{x}) = \mathbf{1}^T \mathbf{R}^{-1} \mathbf{r}(\mathbf{x}) - 1$ .

In Kriging model, the predicted mean value at any point  $\mathbf{x}^i$  in DoE is consistent with the true response value, namely  $\mu_{\hat{G}}(\mathbf{x}^i) = G(\mathbf{x}^i) (i = 1, 2, \dots, m)$ , and the corresponding Kriging variance is null, namely  $\sigma_{\hat{G}}^2(\mathbf{x}^i) = 0 (i = 1, 2, \dots, m)$ . For any point out of DoE, the Kriging variance is not zero, and its value reflects the accuracy of the prediction results at the point. For clarity, **Fig. 1** demonstrates an example of prediction results of Kriging model within the range of [0,10.0], which include  $\mu_{\hat{G}}(x) (x \in [0, 10.0])$  and  $\mu_{\hat{G}} \pm \sigma_{\hat{G}}(x) (x \in [0, 10.0])$ , based on the given sample data in DoE. The Kriging variance of Kriging model provides a basis for selecting representative experimental design points. Generally, learning functions can be constructed according to Kriging variance and predicted mean value to realize active learning based on the current Kriging model, and finally the perfect Kriging model can be established.

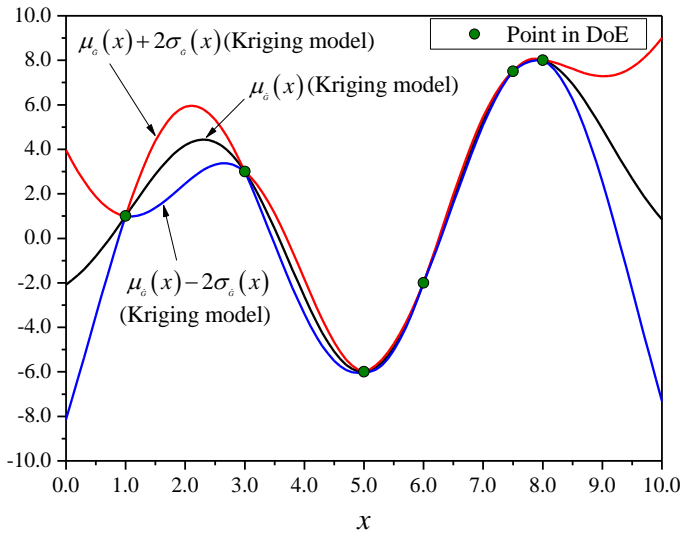


**Fig. 1.** The predicted mean value and Kriging variance of Kriging model.

## 2.2. Implementation of AK-MCS

The Kriging model, based on the given data from the Design of Experiments (DoE), approximates the relationship between sample points and performance function values, and predicts

the shape of the Limit State Function (LSF). By using the established Kriging model as a surrogate model, the failure probability can be determined through Monte Carlo simulation using the following formula:

$$\hat{P}_f = \frac{n_{\hat{G} \leq 0}}{n_{MC}} \quad (9)$$

where  $n_{MC}$  represents the total number of sampling in MCS and  $n_{\hat{G} \leq 0}$  refers to number of sampling with  $\hat{G} \leq 0$  in MCS.

To address the issue of constructing data for DoE, scholars have proposed the adaptive Kriging surrogate model with active learning ability methods. These approaches involve gradually improving the Kriging model through a series of iterative processes. In each iteration, all candidate samples are evaluated using the current Kriging model with a predefined learning function. The sample with the highest (or lowest) value of the learning function is selected and added to DoE for updating the Kriging model. Generally, representative samples contribute more to improving the accuracy of the Kriging model and typically have the following spatial distribution characteristics: (1) representative samples are usually close to the limit state surface; and (2) new representative samples are commonly located in regions where existing DoE samples are relatively sparse due to higher uncertainty.

The learning function is the basis for selecting representative samples. Various learning functions have been developed, including the sign indication learning function (U function) [14], the Expected Feasibility Function (EFF) [36], the information entropy theory-based learning function (H function) [29], and the Least Improvement Function (LIF) [27]. In this paper, the sign indication learning function (U function) used in AK-MCS is employed to guide the selection of representative samples. The U function is constructed based on the risk of crossing the limit state surface and is defined as follows:

$$U(\mathbf{x}) = \frac{|\mu_{\hat{G}}(\mathbf{x})|}{\sigma_{\hat{G}}(\mathbf{x})} \quad (10)$$

According to the definition of the U function, samples with a high probability of crossing the limit state surface are added to the DoE set because the positive and negative signs of their corresponding performance function values are easily influenced by uncertain factors, resulting in changes in failure probability. Therefore, representative samples should be located according to the following conditions: (1) the predicted mean value of the performance function is close to zero; and (2) the Kriging variance of the performance function is relatively high.

In the process of updating the Kriging model, the values of  $U$  function for all candidate samples in CSP  $\mathbf{S}_{pool} = (\mathbf{x}_c^1, \mathbf{x}_c^2, \dots, \mathbf{x}_c^p)$  are firstly calculated using the current Kriging model, and then the sample with lowest  $U$  value among these candidate samples is added to the set of DoE. Hence, the learning criterion is defined as  $\min(U(\mathbf{x})) (\mathbf{x} \in \mathbf{S}_{pool})$ .

The stopping criteria of Kriging model update process in AK-MCS [14] is set to be  $\min(U(\mathbf{x})) \geq 2.0$ , which means a sample is incorrectly classified with a probability of  $\Phi(-2) = 0.023$ . It is considered that the correct rate of the surrogate model's response signs to the Monte Carlo population can be guaranteed if the stopping criteria is met. It is important to note that there may still be deviations between the predicted response values using the surrogate model and the actual response values. This is because the samples of DoE used to generate the surrogate model may be insufficient, preventing the surrogate model from accurately depicting the characteristics of the limit state surface. Therefore, the variation coefficient of failure probability  $V_{\hat{P}_f}$  expressed as follows should be further accessed

$$V_{\hat{P}_f} = \sqrt{\frac{1 - \hat{P}_f}{n_{MC} \hat{P}_f}} \quad (11)$$

When  $V_{\hat{P}_f}$  exceeds the preset limit value, it is considered that the size of the current Monte Carlo population is not large enough, and the number of sampling points in Monte Carlo simulation should be increased. It should be noted that, as introduced in AK-MCS, the Monte Carlo population is also used as the pool of candidate samples, so the scale of the candidate pool increases accordingly. Correspondingly, the set of DoE and Kriging surrogate model are continuously updated.

Ref. [14] provides details on the implementation of AK-MCS. Since representative samples are selected from CSP, the distribution of candidate samples significantly impacts the acquisition of representative samples. Generally, candidate samples are obtained through Monte Carlo sampling according to the distribution parameters of random variables and generally follow a standard normal distribution. Then, the distribution of candidate samples in the edge regions of Monte Carlo sampling is relatively sparse, making it difficult to obtain real representative samples for these regions. Considering that reliability analysis for practical engineering often involves small failure probabilities, where real representative sample points often exist at the sampling edge, large-scale candidate pools are required to ensure that real representative sample points can be found. Additionally, for problems with small failure probabilities, a large-scale Monte Carlo population is

required to meet the limit condition of the variation coefficient of failure probability. In other words, as failure probability decreases, the scale of the Monte Carlo population and candidate pool increases accordingly. It is worth noting that as the scale of the candidate pool increases, so does the computational effort required to evaluate candidate samples using the Kriging surrogate model, ultimately affecting the efficiency of adaptive Kriging surrogate model methods. Therefore, overcoming the limitations of CSP-based methods in selecting representative samples is key for adaptive Kriging surrogate model methods to solve reliability analysis problems with small failure probabilities. The authors believe that using an optimization algorithm to obtain representative samples, rather than the regular CSP-based method, is a promising approach to improving the performance of adaptive Kriging surrogate model methods.

### 3. Improved AK-MCS

By treating the values of random variables as design variables, the selection of representative samples is fundamentally an optimization problem, where the objective is to minimize the value of the function defined in Eq. (10) within a given design space. The objective function is often a nonlinear function with multiple peaks (or valleys). Therefore, conventional optimization algorithms, such as gradient-based methods, may only yield local optima and produce suboptimal results. In contrast, modern optimization algorithms such as Genetic Algorithm (GA), Ant Colony Algorithm (ACA), and Particle Swarm Optimization (PSO) are more appropriate for solving this complex optimization problem, because these algorithms are theoretically capable of finding global optima and do not require the optimized functions to be differentiable or continuous. Given its effectiveness in handling continuous variable optimization and ease of implementation, PSO is employed as the primary algorithm for optimization in the improved AK-MCS proposed. As the selection process for representative samples is no longer dependent on the scale of CSP or the distribution characteristics of random variables, the likelihood of obtaining representative samples is significantly increased. This section introduces the implementation of PSO and the improved CSP-free AK-MCS.

#### 3.1. Implementation of PSO

PSO was originally introduced by Kennedy and Eberhart in 1995 [41]. The algorithm is designed to solve global optimization problems involving nonlinear objective functions with continuous variables. The underlying concept of PSO is inspired by the foraging behavior of birds, where individuals follow the best-performing member of the flock without knowing the exact location or distance to food. In PSO, each potential solution to the optimization problem is represented as a ‘particle’ in the search space. Particles are evaluated based on a fitness function

determined by the objective function and move through the solution space at random speeds. Through information exchange, particles can obtain heuristic information to guide the swarm towards an optimal solution. PSO has been applied in various fields, including structural optimization [42], topology optimization [43], structural reliability evaluation [44] and reliability optimization design [45]. For further developments and applications of PSO, readers are referred to Ref. [39].

An optimization problem with a  $N_D$ -dimension search space can be solved by using PSO with the size of particle swarm (number of particles)  $N_{swarm}$  and the maximum iteration number  $N_{ite\_max}$  predetermined. When the algorithm runs to the  $n^{\text{th}}$  ( $n=1, 2, \dots, N_{ite\_max}$ ) iteration, the current position and current velocity of the  $i^{\text{th}}$  ( $i=1, 2, \dots, N_{swarm}$ ) particle are expressed as  $\mathbf{X}_i^{(n)} = (X_{i,1}^{(n)}, X_{i,2}^{(n)}, \dots, X_{i,N_D}^{(n)})$  and  $\mathbf{V}_i^{(n)} = (V_{i,1}^{(n)}, V_{i,2}^{(n)}, \dots, V_{i,N_D}^{(n)})$ , respectively. Then, for each particle, the following formulas are used to update the speed and position in each dimension component at each iteration.

$$V_{i,j}^{(n+1)} = \omega \cdot V_{i,j}^{(n)} + c_1 \cdot rand \cdot (X_{pbest,i,j}^{(n)} - X_{i,j}^{(n)}) + c_2 \cdot rand \cdot (X_{gbest,j}^{(n)} - X_{i,j}^{(n)}) \quad (j = 1, 2, \dots, N_D) \quad (12)$$

$$X_{i,j}^{(n+1)} = X_{i,j}^{(n)} + V_{i,j}^{(n+1)} \quad (j = 1, 2, \dots, N_D) \quad (13)$$

In Eq. (12),  $\omega$  is the inertia weight,  $c_1$  and  $c_2$  refer to the cognition learning factor and social learning factor, respectively,  $X_{pbest,i,j}^{(n)}$  represents the  $j^{\text{th}}$  component of the historical best position of the  $i^{\text{th}}$  particle at the  $n^{\text{th}}$  iteration,  $X_{gbest,j}^{(n)}$  represents the  $j^{\text{th}}$  component of the best position of the whole swarm at the  $n$  iteration,  $rand$  means to generate a random value uniformly distributed within the range of  $[0,1]$ . For the sake of convenience, the historical best position of a particle and the best position of the whole swarm at the  $n^{\text{th}}$  iteration are expressed as  $\mathbf{X}_{pbest,i}^{(n)} = (X_{pbest,i,1}^{(n)}, X_{pbest,i,2}^{(n)}, \dots, X_{pbest,i,N_D}^{(n)})$  and  $\mathbf{X}_{gbest}^{(n)} = (X_{gbest,1}^{(n)}, X_{gbest,2}^{(n)}, \dots, X_{gbest,N_D}^{(n)})$ , respectively. Generally, the historical best position of a particle  $\mathbf{X}_{pbest,i}^{(n)}$  changes with the iteration process and can be described by

$$\mathbf{X}_{pbest,i}^{(n+1)} = \begin{cases} \mathbf{X}_i^{(n+1)}, & \text{if } F_{\text{fit}}(\mathbf{X}_i^{(n+1)}) > F_{\text{fit}}(\mathbf{X}_{pbest,i}^{(n)}) \\ \mathbf{X}_{pbest,i}^{(n)}, & \text{otherwise} \end{cases} \quad (14)$$

where  $F_{\text{fit}}(\cdot)$  refers to the fitness function. Among the historical best positions of all particles, the best position with the highest fitness value is recorded as the best position of the whole swarm,

expressed as

$$\begin{aligned}\mathbf{X}_{gbest}^{(n)} &\in \left\{ \mathbf{X}_{pbest,1}^{(n)}, \mathbf{X}_{pbest,2}^{(n)}, \dots, \mathbf{X}_{pbest,N_{swarm}}^{(n)} \mid F_{\text{fit}}\left(\mathbf{X}_{pbest,i}^{(n)}\right) \right\} \\ &= \max \left\{ F_{\text{fit}}\left(\mathbf{X}_{pbest,1}^{(n)}\right), F_{\text{fit}}\left(\mathbf{X}_{pbest,2}^{(n)}\right), \dots, F_{\text{fit}}\left(\mathbf{X}_{pbest,N_{swarm}}^{(n)}\right) \right\}\end{aligned}\quad (15)$$

As discussed above, the movement of particles is influenced by three factors. The first is the current speed of motion, which reflects the continuity of particle movement between successive iterations. The second is the particle's historical best position, which reflects the influence of its own experience on its direction of movement. The third is the best position of the swarm, which reflects the influence of the swarm's collective experience on the direction of particle movement.

**Fig. 2** illustrates the motion of a particle.

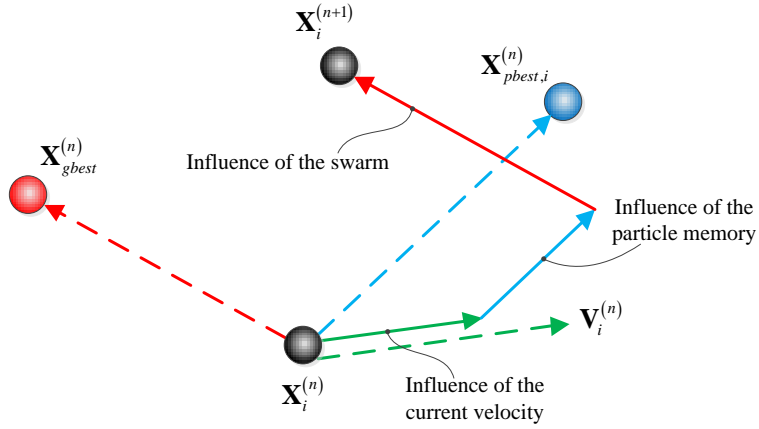


**Fig. 2.** The sketch map of particle motion in PSO [39].

The performance of PSO is influenced by the parameters  $\omega$ ,  $c_1$  and  $c_2$ . The inertia weight  $\omega$  is a parameter that controls the influence of a particle's velocity from the previous iteration. Introduced by Eberhart [44], this parameter affects the balance between global and local search capabilities. A higher inertia weight generally enhances global optimization ability, while a lower inertia weight improves local optimization ability. The value of the inertia weight typically ranges between 0 and 1.0, with a recommended value of 0.729 as suggested by Clerc and Kennedy. Some researchers have also proposed updating strategies that decrease the inertia weight over time. The cognitive learning factor  $c_1$  reflects the influence of the distance between a particle's current position and its historical best position. This means that particles move according to their own cognition. The social learning factor  $c_2$  describes the influence of the distance between a particle's current position and the swarm's best position. This reflects information sharing and cooperation among particles, as well as their tendency to move according to the swarm's collective experience.

Both  $c_1$  and  $c_2$  are typically set to 2.0, with a recommended value of 1.494 as suggested by Clerc and Kennedy [46]. Additionally, a velocity limit constant  $V_{\max}$  is often introduced to control the maximum distance a particle can move in each iteration, thereby controlling the convergence speed and global search ability of the algorithm.

The main steps of PSO used in this work are as follows.

**Step 1:** Set control parameters for PSO, including  $N_{\text{swarm}}$ ,  $N_{\text{ite\_max}}$ ,  $\omega$ ,  $c_1$ ,  $c_2$  and  $V_{\max}$ .

**Step 2:** Initialize the particle swarm by randomly generating the position and velocity of each particle within the solution space. Evaluate all particles in the swarm and set their current position as their historical best position. Determine the swarm's best position according to Eq. (15).

**Step 3:** Update the position and velocity of all particles using Eqs. (12) and (13). Adjust the updated particles according to any constraints and generate a new particle swarm.

**Step 4:** Evaluate all particles in the swarm and determine their historical best position according to Eq. (14). Determine the swarm's best position using Eq. (15).

**Step 5:** If the maximum number of iterations has been reached, output the swarm's best position and end the program. Otherwise, return to **Step 3** and continue.

### 3.2. Implementation of the improved AK-MCS

#### 3.2.1. Optimization model for representative points

Generally, the values of random variables in the standard normal space are regarded as the design variables and denoted as  $\mathbf{X} = (X_1, X_2, \dots, X_{N_D})$ . From the viewpoint of optimization, the next representative sample is determined by solving the following optimization formulation,

$$\begin{aligned} \text{find } \mathbf{X}^* &= (X_1^*, X_2^*, \dots, X_{N_D}^*) \\ \text{min } F_{\text{obj}}(\mathbf{X}) &= \frac{|\mu_{\hat{G}}(\mathbf{X}) - \delta|}{\sigma_{\hat{G}}(\mathbf{X})} + p \cdot \max(|\mathbf{X}| - r_c, 0) \\ \text{s.t. } X_j &\in [-X_{\text{lim}}, X_{\text{lim}}] \quad (j = 1, 2, \dots, N_D) \end{aligned} \quad (16)$$

where  $\mathbf{X}^*$  is the optimum of Eq. (16)  $X_j \in [-X_{\text{lim}}, X_{\text{lim}}] \quad (j = 1, 2, \dots, N_D)$  reflects the search range of the  $j$  design variable,  $\delta$  is a preset small quantity that describes the offset between the search target and the LSF. If no otherwise specified,  $\delta$  is set to be zero. Given that the probability of obtaining samples in  $(-\infty, -6.0)$  and  $(6.0, \infty)$  is extremely small when conducting random sampling according to the standard normal distribution, this paper sets  $X_{\text{lim}} = 6.0$ . In the implementation of PSO, the fitness function can be obtained by  $F_{\text{fit}}(\mathbf{X}) = 1/(F_{\text{obj}}(\mathbf{X}) + \delta_0)$  with

$\delta_0$  the preset small quantity.

In Eq. (16),  $F_{\text{obj}}(\mathbf{X})$  represents the objective function, where  $p \cdot \max(\|\mathbf{X}\| - r_c, 0)$  is a penalty term with  $r_c$  controlling the sampling range and  $p$  representing the penalty intensity, named as penalty coefficient. The purpose of introducing the penalty term is to avoid finding representative sample points outside the given range as far as possible, because these points have little contribution to the construction of high-precision surrogate models. As shown in **Fig. 3**, the edge region of Monte Carlo sampling is actually circular for a problem with two design variables. When calculating failure probability, the contribution of sampling points outside the circular edge to the construction of a high-precision surrogate model typically decreases with increasing distance from the sampling center. Therefore, a hypersphere with a suitable radius  $r_c$  can be predefined. For sampling points outside this hypersphere, a penalty term that increases with the magnitude of the sample point can be introduced to reduce the likelihood of selecting such points. For random variables in standard normal space, the value of the Cumulative Distribution Function (CDF) at -4.30 is as low as  $\Phi(-4.3) = 8.54 \times 10^{-6}$ . Therefore, if no otherwise specified, the radius  $r_c$  is set to  $r_c = 4.30$ , which is sufficient for most problems involving small failure probabilities. For the problem with higher failure probabilities, the radius can be set as a lower value to improve the efficiency in surrogate model construction. The penalty coefficient  $p$  should be set according to the range of performance function values  $G(\mathbf{X})$  within the sampling space. In this work, the penalty coefficient is set as follows:

$$p = \frac{\bar{G}(\mathbf{X})|_{\mathbf{X} \in \text{DoE}} - \underline{G}(\mathbf{X})|_{\mathbf{X} \in \text{DoE}}}{4.0} \quad (17)$$

where  $\underline{G}(\mathbf{X})|_{\mathbf{X} \in \text{DoE}}$  and  $\bar{G}(\mathbf{X})|_{\mathbf{X} \in \text{DoE}}$  represent the minimum and maximum of the performance function values obtained from the current set of DoE. It should be noted that this setting of the penalty coefficient does not strongly restrict representative sample points to within the specified hypersphere. As long as the objective function value is low enough, samples outside the hypersphere can also be selected as representative points, avoiding the potential lack of truly representative sample points due to the limitations of the hypersphere. In fact, for problems involving small failure probabilities, sample points near the hypersphere are also near the limit state surface and play an important role in calculating failure probability using surrogate models.

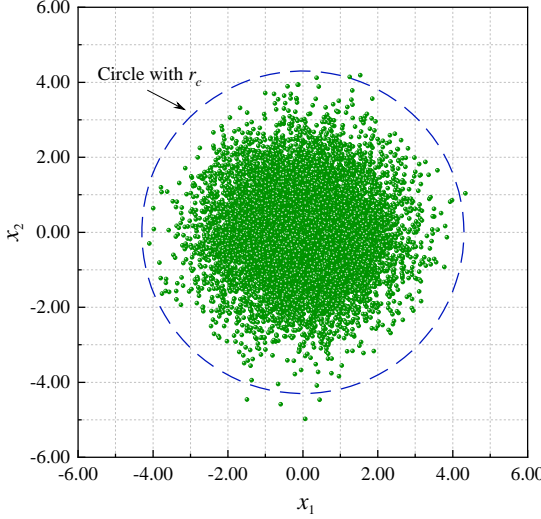


**Fig. 3.** Distribution of sampling points in standard normal space.

### 3.2.2. Implementation of the improved AK-MCS

Different from the regular CSP-based AK-MCS where the CSP varies with Monte Carlo population, the improved CSP-free AK-MCS is implemented through two independent stages: surrogate model construction and MCS with the established surrogate model for estimating the failure probability. The construction of surrogate model is a two-level iterative process. The outer iteration involves gradually increasing the data of DoE and improving the Kriging surrogate model. The inner iteration involves implementing PSO. The maximum iteration number serves as the stopping condition for the inner iteration, while  $\min(U(\mathbf{X})) \geq 2.0$  is the stopping criteria for the outer iteration, which is the same as AK-MCS and detailed in **Sec 2.2**. It is important to note that during the initial stage of constructing the surrogate model, it is possible for model updating to stop if the selected ‘representative sample points’ meet the condition of  $\min(U(\mathbf{X})) \geq 2.0$ , and finally the ideal surrogate model cannot be obtained. This can occur because there may be significant differences between the performance function obtained from the Kriging model based on the initial data of DoE and the real performance function, resulting in false representative samples. To avoid the premature stop of the surrogate model construction, it is required that the set of DoE  $\mathbf{S}_{\text{DoE}}$  contain at least one sample point in the vicinity of the limit state surface. The condition for meeting this requirement is expressed as

$$G(\mathbf{X}) < 0.1 \cdot \|\nabla \hat{G}(\mathbf{X})\| \quad (18)$$

where  $\nabla \hat{G}(\mathbf{X})$  represents the gradient vector of the predicted performance function value to the random variables, which can be obtained by using the Kriging model.

The main steps of the improved CSP-free AK-MCS for reliability analysis are listed as follows:

**Step 1:** Set control parameters for PSO, including  $N_{swarm}$ ,  $N_{ite\_max}$ ,  $\omega$ ,  $c_1$ ,  $c_2$  and  $V_{max}$ .

**Step 2:** Build the initial data of DoE. Generate the initial set of DoE  $\mathbf{S}_{DoE} = (\mathbf{X}^1, \mathbf{X}^2, \dots, \mathbf{X}^m)$

using Latin Hypercube Sampling (LHS) according to the distribution parameters of random variables, and obtain the performance function values of them denoted as  $\mathbf{Y}_{DoE} = (G(\mathbf{X}^1), G(\mathbf{X}^2), \dots, G(\mathbf{X}^m))$  with  $m$  being the number of samples in DoE.

**Step 3:** Construct the Kriging model according to the data in  $\mathbf{S}_{DoE}$  and  $\mathbf{Y}_{DoE}$ .

**Step 4:** Based on the current Kriging model, select a representative sample through PSO, which includes the following sub-steps:

Step 4-(1): Initialization of particle swarm. Generate particle swarm by randomly initializing the position and velocity of each particle in the solution space. Evaluate all particles in the swarm using Eqs. (16) and set the current position as the historical best position for each particle. Meanwhile, determine the swarm's best position according to Eq. (15).

Step 4-(2): Update the position and velocity for all particles using Eqs. (12) and (13) and obtain a new generation of particle swarm.

Step 4-(3): Evaluate all particles in the swarm using Eqs. (16), and update the historical best position for each particle and the best position of the whole swarm using Eqs. (14) and (15). If the iteration number does not reach  $N_{ite\_max}$ , turn to Step 4-(2); otherwise, go to the next step.

Step 4-(4): If the iteration number reaches  $N_{ite\_max}$ , output the best position of the swarm as the selected representative sample point.

**Step 5:** Receive the representative sampling point  $\mathbf{X}^* = \mathbf{X}_{gbest}^{(N_{ite\_max})}$  selected by PSO, and check the condition for stopping update of Kriging model. If  $U(\mathbf{X}^*) \geq 2.0$ , go to **Step 6**; otherwise, obtain the value of performance function  $G(\mathbf{X}^*)$  and add  $\mathbf{X}^*$  and  $G(\mathbf{X}^*)$  to  $\mathbf{S}_{DoE}$  and  $\mathbf{Y}_{DoE}$ , respectively, then turn to **Step 3**.

**Step 6:** Generate Monte Carlo population  $\mathbf{S}_{MC} = (\mathbf{X}^1, \mathbf{X}^2, \dots, \mathbf{X}^{n_{MC}})$  by Monte Carlo sampling according to the random variables in the system with given distribution parameters.

**Step 7:** Predict the mean values of performance function  $u_{\hat{G}}(\mathbf{X}^i) (i=1, 2, \dots, n_{MC})$  for all

samples in the Monte Carlo population  $\mathbf{S}_{MC} = (\mathbf{X}^1, \mathbf{X}^2, \dots, \mathbf{X}^{n_{MC}})$  using the established Kriging surrogate model. Then, the estimated failure probability  $\hat{P}_f$  can be calculated using Eq. (9).

**Step 8:** Check the sufficiency of Monte Carlo population through the variation coefficient of failure probability  $V_{\hat{P}_f}$  obtained using Eq. (11). If  $V_{\hat{P}_f} < 0.05$ , output  $\hat{P}_f$  and end the program. If  $V_{\hat{P}_f} \geq 0.05$ , generate a new batch of samples by Monte Carlo sampling according to the distribution characteristics of random variables, add these samples to Monte Carlo population  $\mathbf{S}_{MC}$ , and then turn to **Step 7**.

**Fig. 4** displays the flow chart of the improved CSP-free AK-MCS. It can be observed that the improved AK-MCS does not require the construction of a CSP. Additionally, there is no need for repeated evaluation of the variation coefficient of failure probability during surrogate model construction. This method clearly separates surrogate model construction and failure probability evaluation into two distinct stages, resulting in a more transparent implementation process. It is important to emphasize that the proposed method selects representative samples based on an optimization algorithm rather than a CSP-based method. This addresses the issue of being unable to obtain representative sample points in sparse distribution regions of candidate samples. With the method proposed in this paper, a Kriging surrogate model for reliability analysis with small failure probability can be constructed without introducing more complex sampling techniques such as importance sampling [23] or subset simulation [7]. This provides a more concise and straightforward approach for reliability analysis.

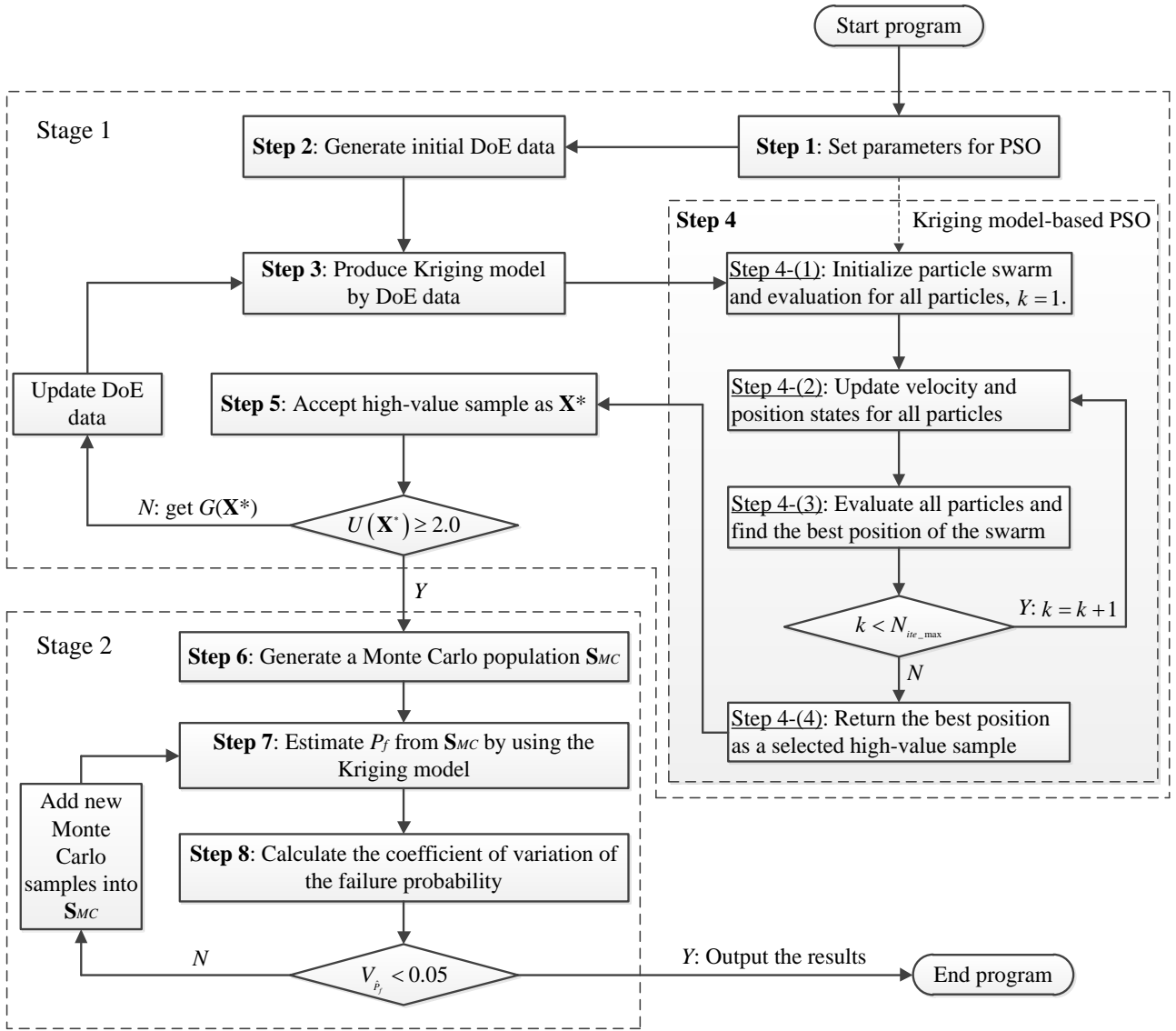


**Fig. 4.** Flow chart of the improved CSP-free AK-MCS.

The representative sample selection and Monte Carlo sampling in the improved AK-MCS are both carried out in standard normal space. The Rosenblatt transformation  $\mathbf{x} = T(\mathbf{X})$  is used to describe the relationship between sample point  $\mathbf{X}$  in standard normal space and sample point  $\mathbf{x}$  in original design space. Thus, the failure probability is rewritten as

$$P_f = \int I_{G<0}(G(\mathbf{X})) f_x(\mathbf{X}) d\mathbf{X} \quad (19)$$

where  $f_x(\mathbf{X})$  is the joint standard normal distribution density function,  $I_{G<0}(G(\mathbf{X}))$  is the failure indicator in the standard normal space determined by the LSF  $G(\mathbf{X}) = G(T^{-1}(\mathbf{x})) = 0$ . The relationship between standard normal space and original design space is shown in **Fig. 5**. Based on the standard normal space, the significance of the distance between two sample points is

independent on the actual distribution of random variables, which is more appropriate to define the distance parameters for construction of learning functions. In standard normal space, the point on the limit state surface  $G(\mathbf{X})=0$  with a smaller distance from the origin in standard normal space represents more important information in estimating the true failure probability, such as the MPP shown **Fig. 5**. Based on the reliability theory, the first-order reliability index  $\beta$  can be obtained according to the distance from MPP to the coordinate origin as  $\beta = \|\mathbf{X}_{\text{MPP}}\|$ .

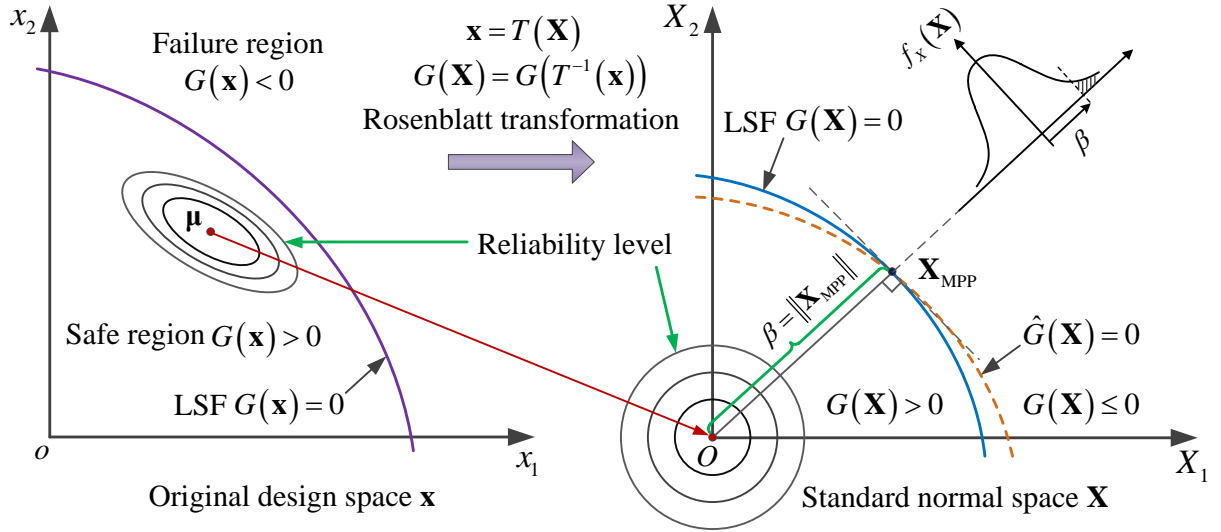


**Fig. 5.** Relationship between  $\mathbf{x}$  space and  $\mathbf{X}$  space.

### 3.2.3. Modification of the objective function

Based on the computational framework of the improved AK-MCS presented in **Sec. 3.2.2**, two issues need to be addressed. The first issue is that the impact of the sample point position is neglected in the evaluation of sample points, which may reduce the efficiency of constructing the surrogate model. For the second issue, the representative samples selected based on the U-function may exhibit a dense distribution in some regions, resulting in a larger scale of DoE. In response to the two issues, the following improvements are proposed.

#### (1) Penalty intensity control

From the viewpoint of reliability analysis, the important degree of sampling points on the LSF is different as the change of their location. Generally, the points closer to the sampling centre in the standard normal space have more important significance. The objective function defined in Eq. (16) does not reflect the impact of the position for the sample points, although a penalty term is used for the sample points outside the hypersphere. Therefore, an additional penalty term is added to the objective function and then the optimization formulation can be rewritten as

$$\text{find } \mathbf{X}^* = (X_1^*, X_2^*, \dots, X_{N_D}^*)$$

$$\min F_{\text{obj}}(\mathbf{X}) = \frac{|\mu_{\hat{G}}(\mathbf{X}) - \delta|}{\sigma_{\hat{G}}(\mathbf{X})} + p \cdot \max(\|\mathbf{X}\| - r_c, 0) + p \cdot \max(\|\mathbf{X}\| - r, 0) \quad (20)$$

$$\text{s.t. } X_j \in [-X_{\text{lim}}, X_{\text{lim}}] (j = 1, 2, \dots, N_D)$$

where  $r$  is a quantity to determine the distribution of penalty intensity. In the initial state of surrogate model construction,  $r$  is obtained as

$$r = r_0 = \frac{1}{m} \sum_{i=1}^m \|\mathbf{X}^i\| \quad (\mathbf{X}^i \in \mathbf{S}_{\text{DoE}}) \quad (21)$$

During the construction of surrogate model,  $r$  is determined as

$$r = \min(\max(\|\mathbf{X}^i\|), r_c) \quad (\mathbf{X}^i \in \mathbf{S}_{\text{DoE}}) \quad (22)$$

Then, the surrogate model construction can be completed when the stopping criteria of  $\min(U(\mathbf{X})) \geq 2.0$  and  $r = r_c$  are reached. For clarity, the sketch map of penalty intensity distribution in the objective function with two design variables is shown in **Fig. 6**.

As mentioned above,  $r$  increases gradually during the construction of the surrogate model. From the perspective of calculation logic, under the premise that there are enough sample points near the sampling center, it is necessary to gradually relax the restrictions on sample points far from the sampling center in order to further capture points on the limit state function and establish an optimization process that expands the search range. This improvement adaptively expands the range of obtaining representative sample points during surrogate model construction, increasing the likelihood of obtaining representative sample points and ensuring the stability of DOE. The effectiveness of this improvement will be verified in the validation section.

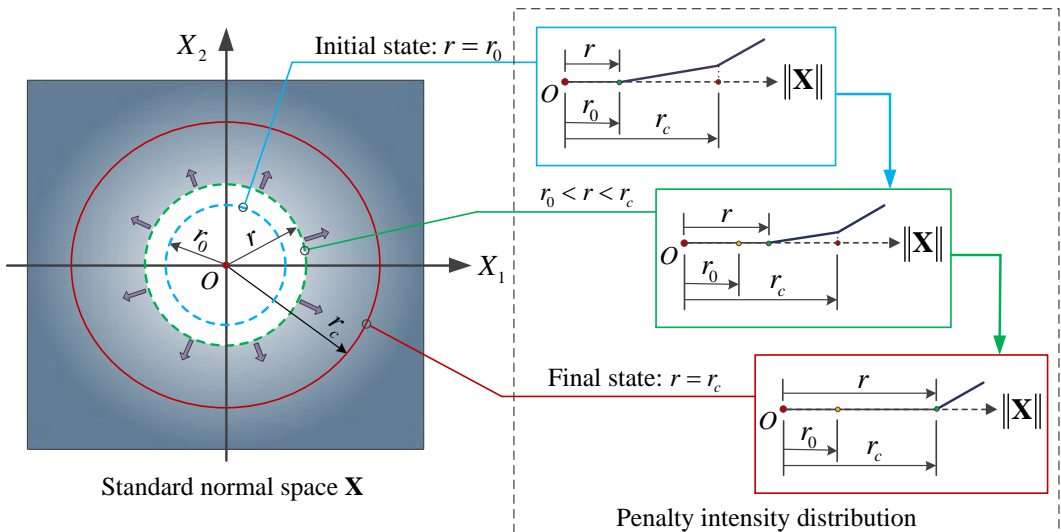


**Fig. 6.** Penalty intensity distribution in the improved AK-MCS.

## (2) Density control

The optimization capability of PSO allows the improved AK-MCS to generate new sample points with lower value of  $U(\mathbf{X})$  compared to the CSP-based AK-MCS. As a result, it is more challenging for the representative samples generated to meet the stopping criteria of  $\min(U(\mathbf{X})) \geq 2.0$ , potentially increasing the final size of DoE. On the other hand, according to the current definition of the U-function, there are points within the given design space with extremely low value of  $U(\mathbf{X})$  despite their limited contribution to improving surrogate model accuracy. In the improved AK-MCS, these points may be discovered through optimization algorithms, increasing the size of DoE.

This issue is illustrated using the performance function  $G(x) = \sin(x)$ ,  $x \in [\pi/2, 5\pi/2]$  for better understanding. Assuming that the determined samples of DoE are located at  $x=4.0, 6.18, 6.38$ , and  $7.5$ , a Kriging model is constructed based on these samples and the next representative sample point is located according to the current Kriging model. **Fig. 7** displays the curves of  $\mu_{\hat{G}}(x)$ ,  $\mu_{\hat{G}}(x) \pm \sigma_{\hat{G}}(x)$  and  $U(x)$  (expressed by  $\log_{10} U(x)$ ) based on the current Kriging model. From the figure, it can be observed that the minimum value of  $U(x)$  appears near  $x^* = 2\pi$  in the current state. In other words, even though the DoE samples already contain the two points near  $x^* = 2\pi$  ( $x = 6.18$  and  $x = 6.38$ ), resulting in a very small Kriging variance  $\sigma_{\hat{G}}^2(x)$  in this narrow range, the minimum value remains in this range (point A in the figure) due to the existence of  $\mu_{\hat{G}}(x) = 0$  between  $x = 6.18$  and  $x = 6.38$ . An effective optimization algorithm can identify point A and add it to DoE. However, the Kriging surrogate model constructed based on the new DoE data still shows an extremely low value of  $U(x)$  near point A. In fact, when points at  $x = 6.18$  and  $x = 6.38$  are included in DoE, point A's contribution to the Kriging model is quite limited. For the current Kriging model shown in **Fig. 5**, point B is a valuable sample point due to its high Kriging variance and low absolute value of the predicted mean  $|\mu_{\hat{G}}(x)|$ . Assuming that point B can be selected and added to DoE, the subsequent Kriging model has a minimum value near point C. Thus, a point near point C can be identified as a representative sample point in the following process. After adding this sample point to DoE, the established Kriging model performs well in distinguishing between failure and safe regions.

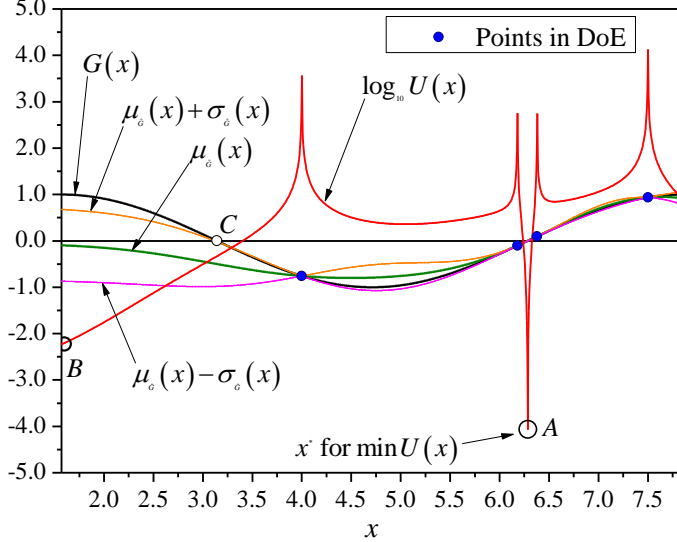


**Fig. 7.** Graphics for discussion on the learning function  $U$ .

As depicted in **Fig. 7**, the points which exhibit a minimum value of  $U(x)$  but lack effective contribution for constructing a surrogate model are usually situated in the immediate vicinity of the existing DOE sample points. To circumvent this issue, it is proposed that the next representative sample to be found should maintain a certain distance from the existing DOE sample points. Therefore, the density control for distance constraint is introduced to avoid overly dense distribution of sample points in DoE. Then, the optimization formulation can be further rewritten as

$$\begin{aligned} \text{find } \mathbf{X}^* &= \left( X_1^*, X_2^*, \dots, X_{N_D}^* \right) \\ \min \quad F_{\text{obj}}(\mathbf{X}) &= \frac{\|\mu_{\hat{G}}(\mathbf{X}) - \delta\|}{\sigma_{\hat{G}}(\mathbf{X})} + p \cdot \max(\|\mathbf{X}\| - r_c, 0) + p \cdot \max(\|\mathbf{X}\| - r, 0) + 2.0c \\ \text{s.t. } X_j &\in [-X_{\text{lim}}, X_{\text{lim}}] \quad (j = 1, 2, \dots, N_D) \end{aligned} \quad (23)$$

where

$$c = \begin{cases} 0, & \|\mathbf{X} - \mathbf{X}^i\| \geq d_c \quad \text{for } \mathbf{X}^i \in \mathbf{S}_{\text{DoE}} \\ 1.0, & \text{otherwise} \end{cases} \quad (24)$$

In Eq. (24),  $d_c$  represents the density control index, and it is determined as

$$d_c = \begin{cases} r_d, & \|\mathbf{X}\| \leq 1/(2r_d) \\ 1.0/(2.0\|\mathbf{X}\|), & \|\mathbf{X}\| > 1/(2r_d) \end{cases} \quad (25)$$

where  $r_d$  represents a parameter used to describe the distance constraint. If no otherwise specified,  $r_d$  is set to be 0.5. The modified objective function in Eq. (23) can be interpreted as augmenting the learning function value by 2.0 when the distance between the position of point  $\mathbf{X}$  and any sample

$\mathbf{X}^i$  in the current DOE is less than the density control index  $d_c$ . For clarity, the definition of density control index is shown in **Fig. 8**. According to the definition in Eq. (25), the value of density control index  $d_c$  decreases with the increase of the distance between the sample point and the sampling center. The purpose of this setting is to relax the density limit of DOE samples in the regions far away from the sampling center, so that more dense DOE sample points can be obtained in these regions to ensure that the surrogate model has sufficient precision for small failure probability problems.

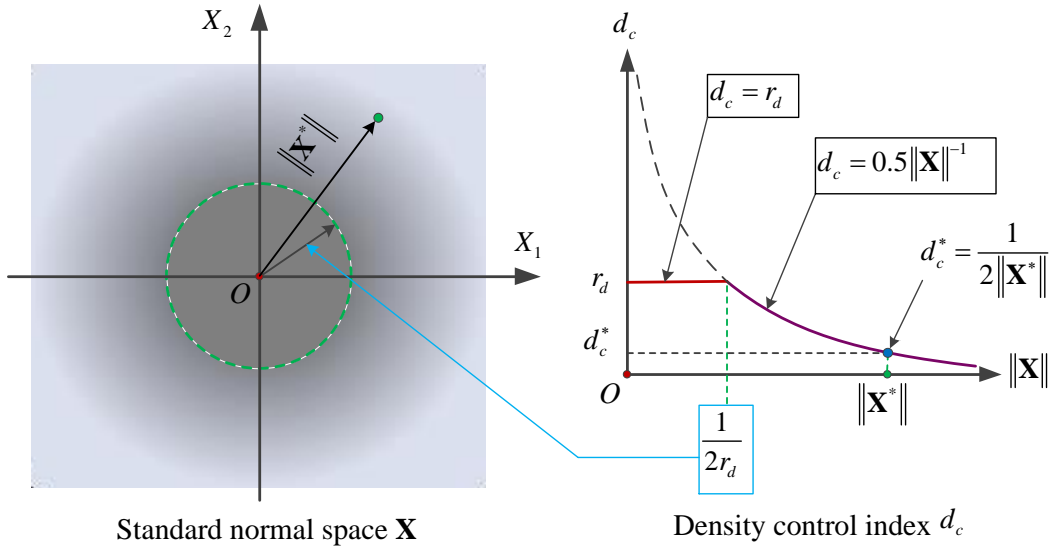


**Fig. 8.** Setting of density control index for DoE.

#### 4. Academic validation

In this section, the computational performance of the proposed method is evaluated through a series of numerical examples. The first example employs a classical series system with four branches to investigate the basic performance of the proposed method and the impact of penalty intensity control and density control. The second example employs a series system with two branches to evaluate the performance of the proposed method for small failure probability problems with disconnected failure regions. The third example considers the modified Rastrigin function with non-convex and scattered gaps of failure domains. The fourth example is a highly nonlinear problem, while the fifth example considers the issue of small failure probability and multiple random variables.

For convenience, the improved CSP-Free AK-MCS based on Eq. (16), Eq. (20) and Eq. (23) are denoted as CFAK-MCS<sup>b</sup>, CFAK-MCS<sup>p</sup> and CFAK-MCS<sup>c</sup>, respectively. The subscripts b, p and c on CFAK-MCS refer to the basic form, the form with penalty intensity control only and the complete form with both penalty intensity control and density control. In the first two examples,

CFAK-MCS<sup>b</sup>, CFAK-MCS<sup>p</sup> and CFAK-MCS<sup>c</sup> are used to investigate the computational performance of the CFAK-MCSs with different definitions of objective functions. The 3<sup>rd</sup>-5<sup>th</sup> examples are conducted to compare CFAK-MCS<sup>c</sup> with other existing methods. To demonstrate the robustness of CFAK-MCS<sup>c</sup>, the reported results in the 3<sup>rd</sup>-5<sup>th</sup> examples are averaged over 50 repeated runs of the algorithm, including failure probability, reliability index, number of performance functional calls in the whole learning process, relative error of failure probability estimation, and coefficient of variation of failure probability.

The solution algorithms have been programmed in MATLAB and run on a computer having an Intel® Core™ i7-8700 processor and a CPU at 3.2GHz with 64GB of RAM.

#### 4.1. Example 1: Series system with four branches

A series system with four branches is employed to investigate the effectiveness of the PSO algorithm in identifying representative samples and to evaluate the influence of utilizing the modified objective functions on the CPAK-MCSs. The performance function of the system is shown in Eq. (26), where  $x_1$  and  $x_2$  are independent standard normal distributed random variables.

$$G(x_1, x_2) = \min \left\{ \begin{array}{l} 3.0 + 0.1 \times (x_1 - x_2)^2 - (x_1 + x_2) / \sqrt{2} \\ 3.0 + 0.1 \times (x_1 - x_2)^2 + (x_1 + x_2) / \sqrt{2} \\ (x_1 - x_2) + 6.0 / \sqrt{2} \\ (x_2 - x_1) + 6.0 / \sqrt{2} \end{array} \right\} \quad (26)$$

##### (1) Effectiveness of PSO

The failure probability of Example 1 is evaluated using both the crude Monte Carlo Simulation (MCS) method and CFAK-MCS<sup>b</sup>. In MCS, random sampling is conducted according to the standard normal distribution and the Monte Carlo population is set to  $1 \times 10^6$ . In CFAK-MCS<sup>b</sup>, the control parameters for PSO are set to  $N_{\text{swarm}} = 50$ ,  $N_{\text{ite\_max}} = 50$ ,  $V_{\max} = 0.3$ ,  $\omega = 0.729$  and  $c_1 = c_2 = 2.0$ . Generally, the optimization ability of PSO increases with the increase of  $N_{\text{swarm}}$  and  $N_{\text{ite\_max}}$ . Based on the previous experience, these settings ensure that PSO has sufficient optimization ability. The number of samples for the initial DoE is set to 6. In the second stage to determine the failure probability, the scale of Monte Carlo population  $\mathbf{S}_{MC}$  is initially set to  $\text{size}(\mathbf{S}_{MC}) = 5 \times 10^4$ . If it is determined that the Monte Carlo population is insufficient when checking its sufficiency of  $V_{\hat{P}_f} \geq 0.05$ , an additional  $5 \times 10^4$  samples are generated and add to  $\mathbf{S}_{MC}$ .

**Table 1** presents the results obtained by using MCS and CFAK-MCS<sup>b</sup>, where  $\hat{P}_f$  refers to the

estimated failure probability,  $N_G$  represents number of calling the real performance function,  $\varepsilon_{\hat{P}_f}$  represents the relative error of failure probability between surrogate model methods and MCS, calculated as

$$\varepsilon_{\hat{P}_f} = \frac{|\hat{P}_{f,\text{surrogate}} - \hat{P}_{f,\text{MCS}}|}{\hat{P}_{f,\text{MCS}}} \times 100\% \quad (27)$$

where  $\hat{P}_{f,\text{MCS}}$  is the estimated failure probability obtained by MCS and  $\hat{P}_{f,\text{surrogate}}$  represents the estimated failure probability obtained by a surrogate model method. As shown by **Table 1**, CFAK-MCS<sup>b</sup> achieves satisfactory accuracy. The number of calling the real performance function in CFAK-MCS<sup>b</sup> is 171, and the relative error of the failure probability is only 0.057%.

**Table 1** Failure probability of Example 1.

Method	$\hat{P}_f / 10^{-2}$	$\varepsilon_{\hat{P}_f} / \%$	$N_G$
MCS	0.4341	-	$1 \times 10^6$
CFAK-MCS <sup>b</sup>	0.4339	0.057	171

**Fig. 9** illustrates the changes of predicted LSF determined by CFAK-MCS<sup>b</sup> when the sample number in DoE (denoted as  $N_{\text{DoE}}$ ) is 21, 36, 51, and 171, respectively. The red dotted line represents the real limit state curves corresponding to the real LSF, while the blue line represents the limit state curves corresponding to the predicted LSF determined by the surrogate model. The star points represent the initial sample points generated by LHS and the round white points represent the sample points added during the process of updating surrogate model. It can be seen that, as  $N_{\text{DoE}}$  increases, the predicted LSF become increasingly closer to the real LSF. Finally, the failure and safe points are accurately distinguished by the predicted limit state curves, as shown in **Fig. 10**.

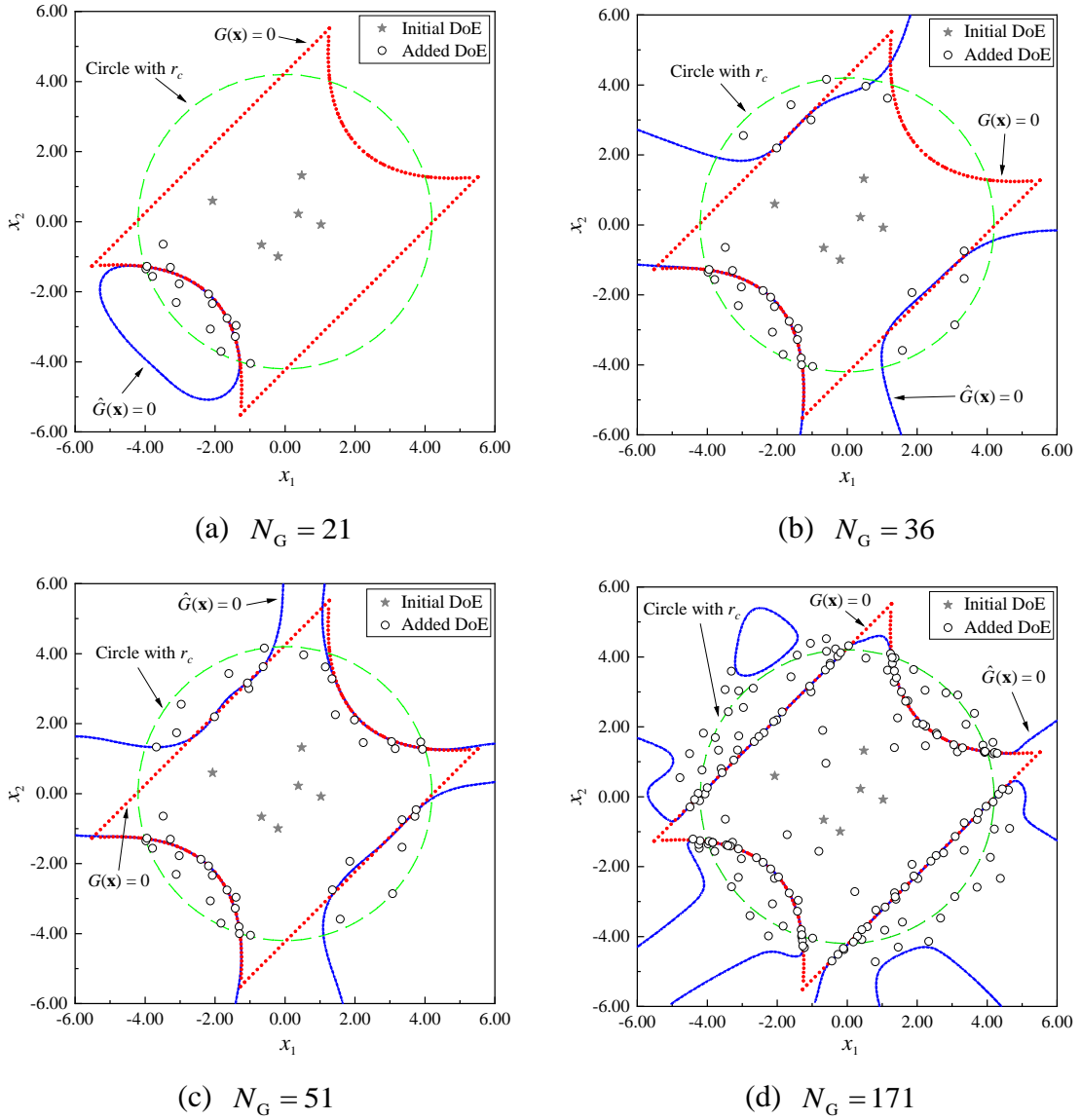


**Fig. 9.** The predicted LSF of CFAK-MCS<sup>b</sup> in evolution process.

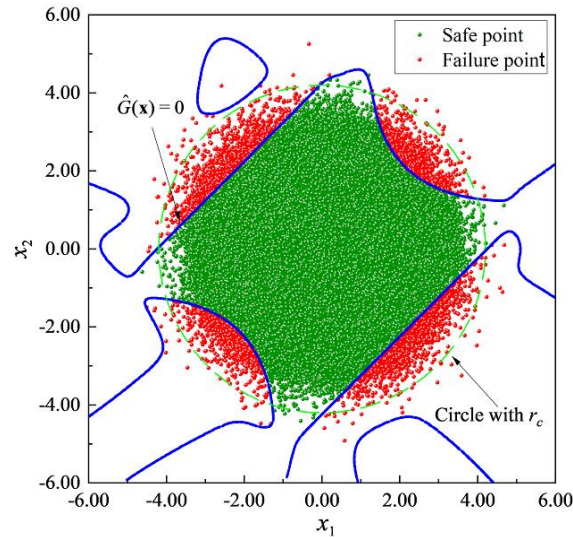


**Fig. 10.** Predicted LSF and the distribution of safe and failure points.

Unlike the CSP-based AK-MCS, CFAK-MCS<sup>b</sup> obtains representative samples through intelligent search based on PSO. **Fig. 11** illustrates the relationship between the sample points in DoE and the objective function value during the construction of the surrogate model in CFAK-MCS<sup>b</sup>. It specifically describes the distribution of the objective function value when the size of DoE is 21, 36, 51, and 171. The representative sample points (green points) found using PSO are located in positions where the objective function value is smaller (dark blue region) under the prediction of the current surrogate model. This verifies the effectiveness of PSO optimization process. Furthermore, the selection of a single representative sample point using PSO is investigated. **Fig. 12** shows the details of obtaining the 21<sup>th</sup> DoE sample point, including the distribution of initially generated particles and their distribution after 15, 30, and 50 iterations. The red arrows depict the motion direction of particles in the next iteration. As iterations progress, particles move closer together and eventually obtain the best position of the swarm in a region with a relatively dense distribution of particles. This indicates the effectiveness of PSO in the proposed methods.

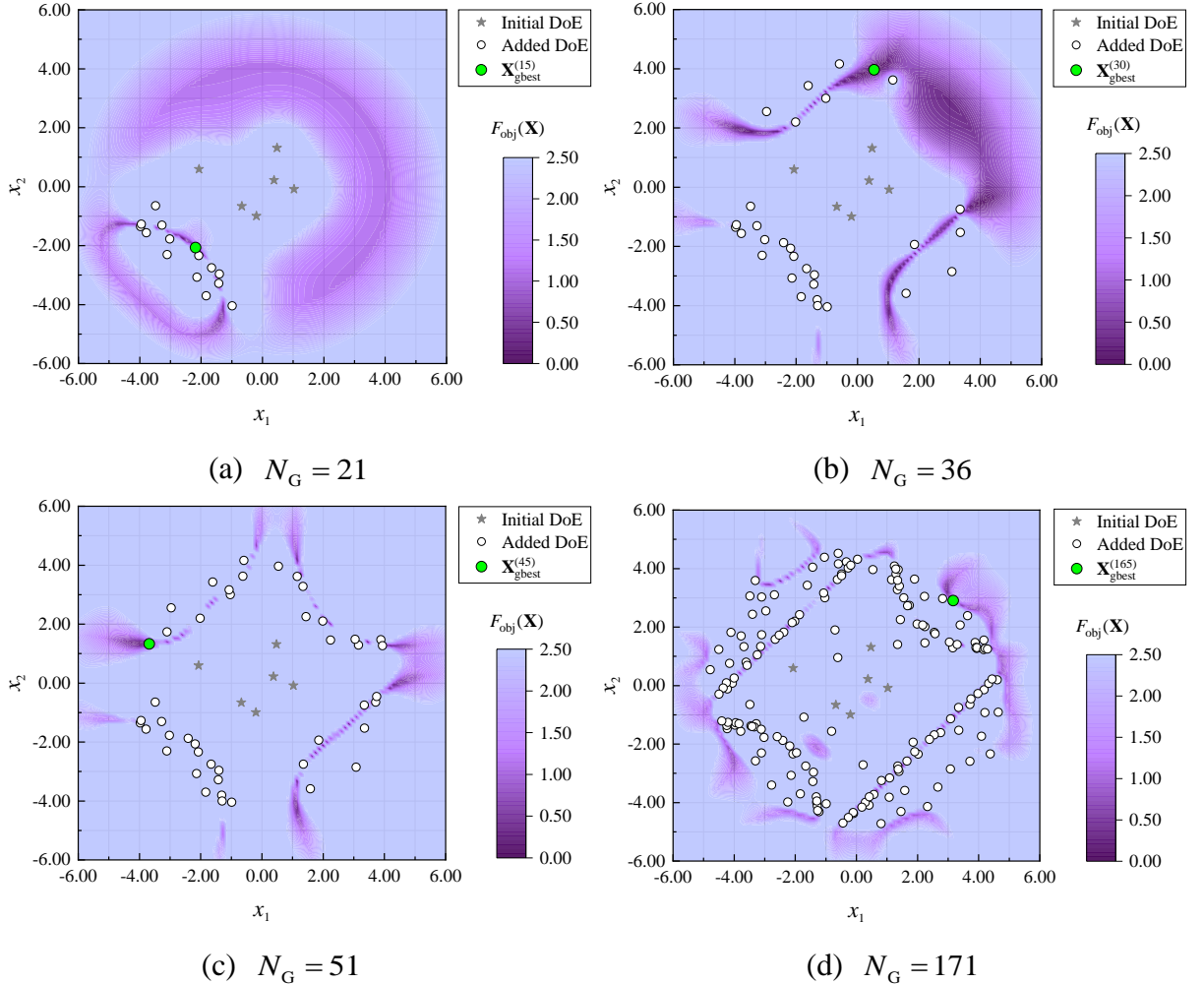


**Fig. 11.** Distribution of objective function and representative sample points.

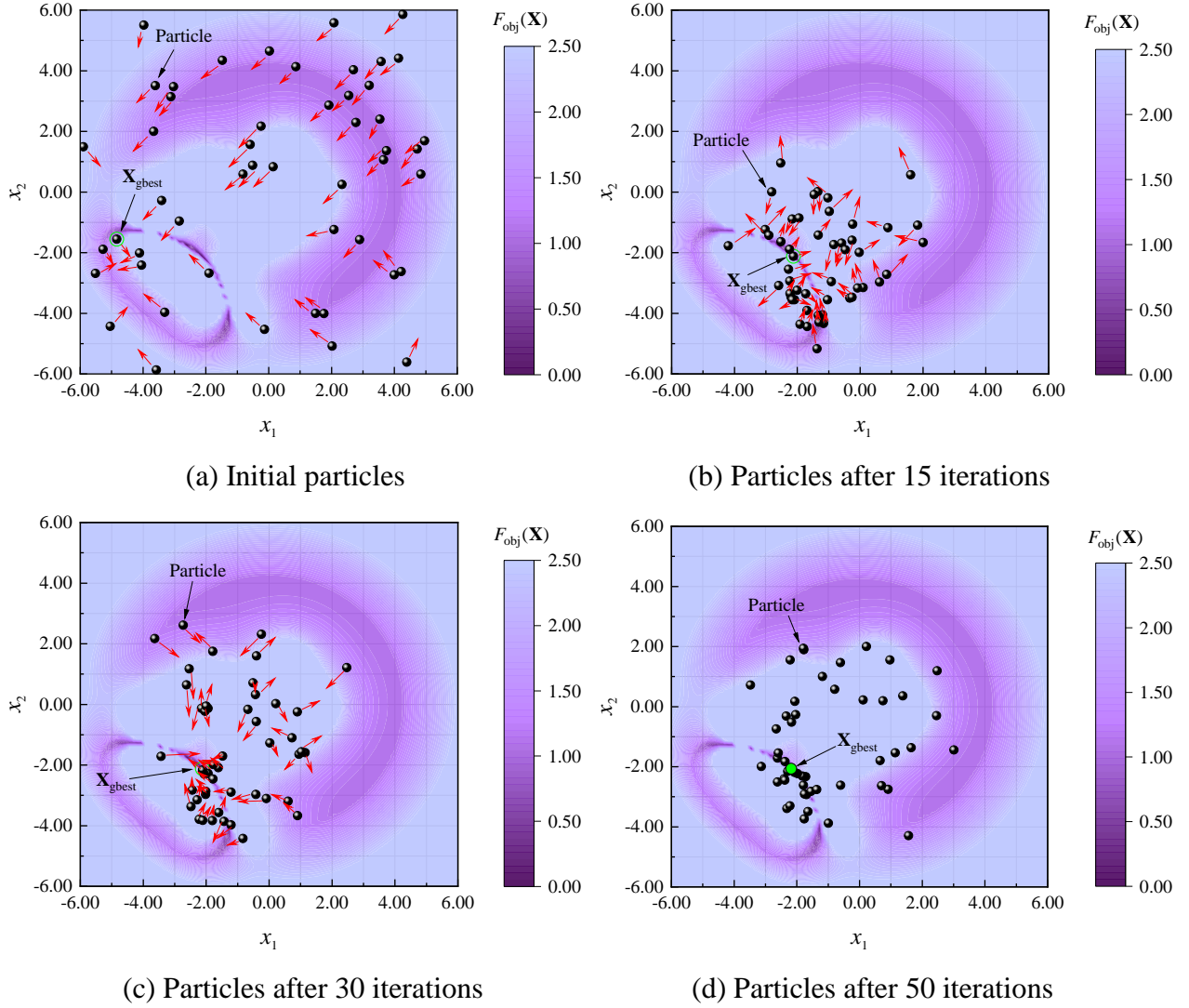


**Fig. 12.** Demonstration of PSO optimization process for the 21<sup>th</sup> point.

## (2) Impact of penalty intensity control and density control

In this section, the impact of penalty intensity control and density control on the performance of CFAK-MCSs is further investigated. Firstly, CFAK-MCS<sup>b</sup>, CFAK-MCS<sup>p</sup> and CFAK-MCS<sup>c</sup> with  $r_d = 0.5$  are used to calculate the failure probability for the series system with four branches (Eq. (26)). A set of results obtained using MCS, CFAK-MCS<sup>b</sup>, CFAK-MCS<sup>p</sup> and CFAK-MCS<sup>c</sup> is shown in **Table 2**. The results show that the number of calling real performance function in CFAK-MCS<sup>p</sup> and CFAK-MCS<sup>c</sup> is significantly reduced comparing to that of CFAK-MCS<sup>b</sup>, and the three surrogate model methods have similar solution accuracy. It indicates that the introduction of penalty intensity control can improve the ability to obtain representative sample points, thus significantly reducing the size of DOE. Compared to CFAK-MCS<sup>p</sup>, the size of DoE for CFAK-MCS<sup>c</sup> is further

reduced, indicating that density control can further improve computational efficiency. In this set of results, 82 DOE samples are sufficient for CFAK-MCS<sup>c</sup> to construct ideal surrogate model. To be more intuitive, **Fig. 13** shows the DoE and predicted LSF during the construction of surrogate model. It can be seen that most DoE points are near the real LSF, so they have an important contribution to the accuracy of the surrogate model. The predicted LSF obtained from the completed surrogate model is very close to the real LSF, so it is can accurately distinguish between safety points and failure points.

Considering the randomness included in the proposed methods, 50 runs are carried out to ensure the reference of the results. **Table 3** lists the statistical results of 50 runs and results from some references. The failure probability of MCS is used to calculate the relative errors of failure probabilities for various methods. In **Table 3**,  $\bar{N}_G$  represents the average number of calling real performance function for construction of the surrogate models,  $\mu_{\hat{P}_f}$  and  $\sigma_{\hat{P}_f}$  represent the average and standard deviation of the failure probabilities obtained from the 50 runs, respectively,  $\bar{\varepsilon}_{\hat{P}_f}$  refers to the average relative error of failure probability between the surrogate model methods and MCS, defined as

$$\bar{\varepsilon}_{\hat{P}_f} = \frac{1}{50} \sum_{i=1}^{50} \varepsilon_{\hat{P}_f}^{(i)} \quad (28)$$

where  $\varepsilon_{\hat{P}_f}^{(i)} (i=1, 2, \dots, 50)$  is the relative error of failure probability for the  $i^{\text{th}}$  run, expressed as

$$\varepsilon_{\hat{P}_f}^{(i)} = \frac{|\hat{P}_{f,\text{surrogate}}^{(i)} - \hat{P}_{f,\text{MCS}}^{(i)}|}{\hat{P}_{f,\text{MCS}}^{(i)}} \times 100\% \quad (29)$$

To be more intuitive, **Fig. 14** shows the size of DoE and relative error of failure probability  $\varepsilon_{\hat{P}_f}^{(i)}$  for the 50 runs carried out by using CFAK-MCS<sup>c</sup>. It can be seen that the maximum relative error does not exceed 1.0%, while the maximum size of DoE does not exceed 160.

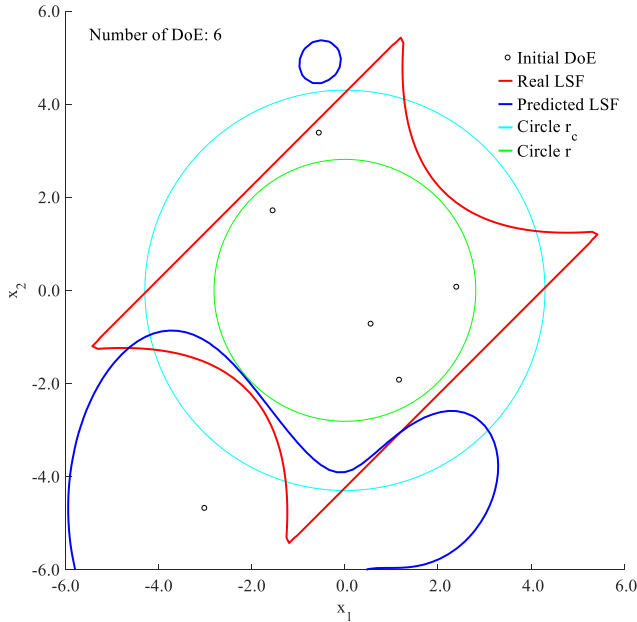
**Table 2** Failure probability of Example 1 obtained by CFAK-MCSs.

Method	$P_f / 10^{-2}$	$\varepsilon_{P_f} / \%$	$N_G$
MCS	0.4436	-	$1 \times 10^6$
CFAK-MCS <sup>b</sup>	0.4434	0.041	189
CFAK-MCS <sup>p</sup>	0.4433	0.068	100
CFAK-MCS <sup>c</sup>	0.4431	0.113	82

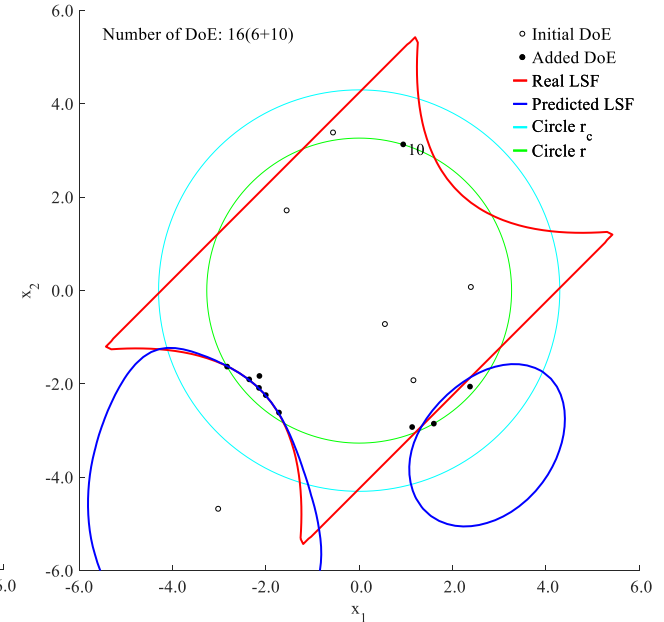
As shown by **Table 3**, CFAK-MCS<sup>b</sup> has extremely high accuracy but a relatively large DOE size. For the three methods of CFAK-MCS<sup>b</sup>, CFAK-MCS<sup>p</sup>, and CFAK-MCS<sup>c</sup>, their computational efficiency improves sequentially, which is reflected in the changes in the size of DOE. It can be considered that the introduction of penalty intensity control and density control plays an important role in improving the efficiency of surrogate model construction. Although the solution accuracy will be reduced after the introduction of penalty intensity and density control, the relative errors of failure probability obtained from CFAK-MCS<sup>p</sup> and CFAK-MCS<sup>c</sup> are both in a satisfactory range. Compared with the existing AK-MCS methods, CFAK-MCS<sup>p</sup> and CFAK-MCS<sup>c</sup> have higher accuracy. From the perspective of algorithm performance, CFAK-MCS<sup>c</sup> can achieve a satisfactory balance between solution accuracy and efficiency.

**Table 3** Summary of the results for Example 1 (50 runs).

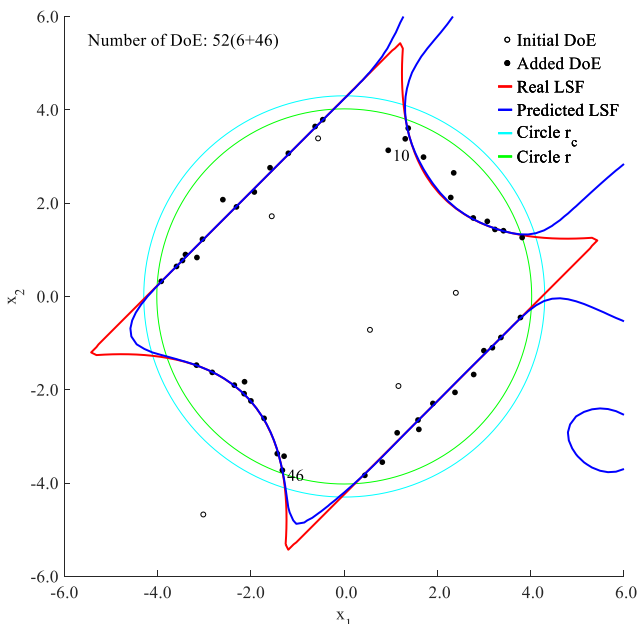
Method	$\mu_{\hat{P}_f} / 10^{-2}$	$\sigma_{\hat{P}_f} / 10^{-4}$	$\bar{\varepsilon}_{\hat{P}_f} / \%$	$\bar{N}_G$
MCS	0.44454	0.6978	-	$1 \times 10^6$
CFAK-MCS <sup>b</sup>	0.44450	0.7025	0.056	182.4
CFAK-MCS <sup>p</sup>	0.44436	0.7116	0.092	114.4
CFAK-MCS <sup>c</sup>	0.44441	0.6825	0.131	94.8
AK-MCS+U [14]	0.4416	-	0.650	126
AK-MCS+EFF [14]	0.4412	-	0.740	124
Directional Sampling (DS) [47]	0.45	-	1.228	52
DS+Nerual Network [47]	0.41	-	7.770	165



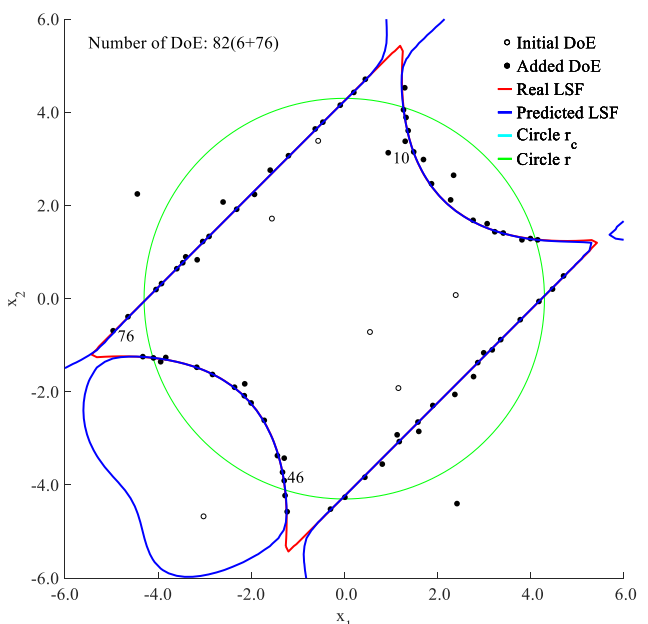
(a)  $N_G = 6$



(b)  $N_G = 16$



(c)  $N_G = 52$



(d)  $N_G = 82$

**Fig. 13.** The predicted LSF and DoE of CFAK-MCS<sup>c</sup> in evolution process.

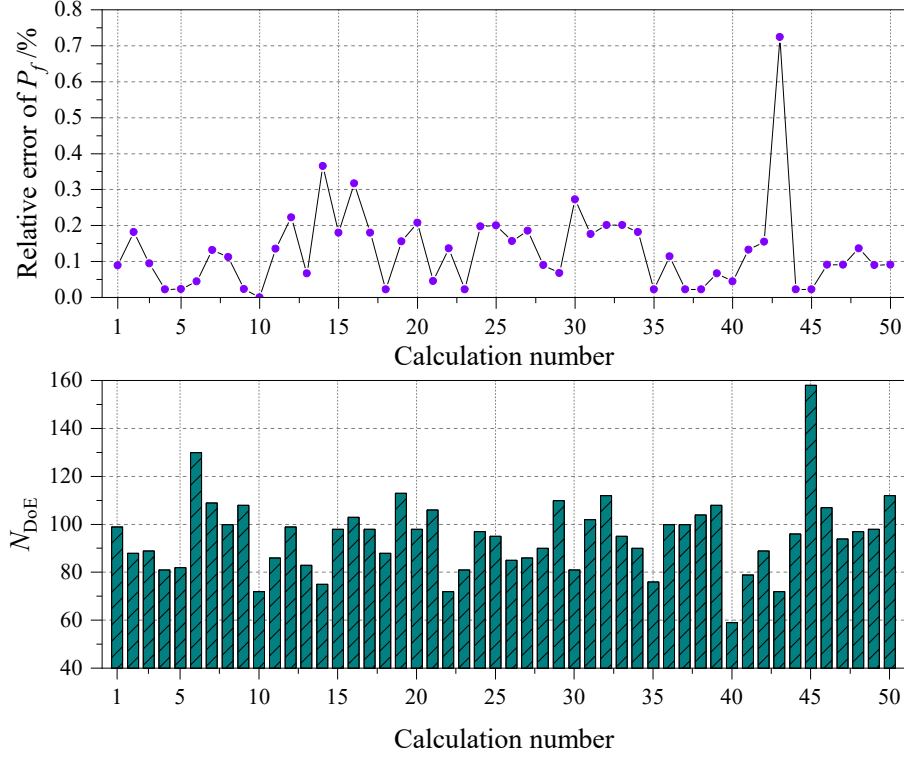


**Fig. 14.** Number of DoE and  $\varepsilon_{\hat{P}_f}$  for CFAK-MCS<sup>c</sup> (50 runs).

#### 4.2. Example 2: Series system with two branches

A series system with two branches is used to show the superiority of the proposed method in small failure probability problems with disconnected failure regions. The performance function of this system is shown in Eq. (30), where  $x_1$  and  $x_2$  are independent standard normal distributed random variables, and  $k$  is a parameter to control the failure probability.

$$G(x_1, x_2) = \min \begin{cases} k + 0.1 \times (x_1 - x_2)^2 - (x_1 + x_2) / \sqrt{2} \\ k + 0.1 \times (x_1 - x_2)^2 - (x_1 + x_2) / \sqrt{2} \end{cases} \quad (30)$$

This study evaluates the cases of  $k = 3.4$  and  $k = 3.9$ . The failure probability of the system is obtained using MCS, AK-MCS [30] and the CFAK-MCSs.

In MCS, the Monte Carlo populations are set to  $1 \times 10^6$  and  $8 \times 10^6$  for the cases of  $k = 3.4$  and  $k = 3.9$ , respectively. In AK-MCS, the number of samples in the initial DoE is set to 6. The size of Monte Carlo population  $S_{MC}$  at the start is set to  $\text{size}(S_{MC}) = 5 \times 10^4$ . If  $V_{\hat{P}_f} \geq 0.05$  when checking the sufficiency of the Monte Carlo population, an additional  $5 \times 10^4$  samples are generated and add to  $S_{MC}$ . The failure probabilities for the two cases are obtained by evaluating the  $1 \times 10^6$  and  $8 \times 10^6$  samples in MCS using the established Kriging surrogate model. In the proposed methods

(CFAK-MCS<sup>b</sup>, CFAK-MCS<sup>p</sup> and CFAK-MCS<sup>c</sup>), the control parameters for PSO are set to  $N_{\text{swarm}} = 100$ ,  $N_{\text{ite\_max}} = 50$ ,  $V_{\text{max}} = 0.3$ ,  $\omega = 0.729$  and  $c_1 = c_2 = 2.0$ . Especially,  $r_d = 0.5$  is used for CFAK-MCS<sup>c</sup>. For the second stage of CFAK-MCSs,  $1 \times 10^6$  and  $8 \times 10^6$  samples in MCS are evaluated using the established surrogate model to estimate the failure probabilities for the two cases, respectively. To ensure the reliability of the results, 50 runs are carried out for each case.

For the two cases, the statistical results of 50 runs are summarized in **Table 4** and **Table 5**, where  $\bar{N}_{\text{EST}}$  represents the average number of predicting the performance function value during the construction of the surrogate models,  $\bar{T}$  is the average CPU time and  $\bar{\varepsilon}_{\hat{P}_f}$  refers to the average relative error of failure probability between the surrogate model methods and MCS.

Under the setting of  $k = 3.4$ , the system's failure probability is about  $4.30 \times 10^{-4}$ . As shown in **Table 4**, both AK-MCS and the CFAK-MCSs achieve high accuracy, with the average errors in failure probabilities within 0.3%. The number of DoE samples required to construct the surrogate model in CFAK-MCS<sup>b</sup> is greater than that of AK-MCS. This can be attributed to the optimization algorithm's ability to find points with lower objective function value in the design space, thus delaying the surrogate model's construction process. In terms of CPU time, CFAK-MCS<sup>b</sup> takes significantly less time than AK-MCS due to the difference in the number of performance function value predictions. In each run, AK-MCS predicts approximately  $1.460 \times 10^7$  performance function values while CFAK-MCS<sup>b</sup> predicts only about  $1.75 \times 10^5$ , resulting in significantly less time consumption for CFAK-MCS<sup>b</sup>. By using the CFAK-MCS<sup>p</sup> and CFAK-MCS<sup>c</sup>, the number of DoE samples required for constructing the surrogate model can be further reduced to be less than that of AK-MCS while maintaining an acceptable relative error in failure probability. In other words, the performance of CFAK-MCS<sup>p</sup> and CFAK-MCS<sup>c</sup> is superior to AKMCS in both computational accuracy and efficiency.

**Table 4** Results of Example 2 for the case of  $k = 3.4$  (50 runs).

Method	$\mu_{\hat{P}_f} / 10^{-4}$	$\sigma_{\hat{P}_f} / 10^{-4}$	$\bar{\varepsilon}_{\hat{P}_f} / \%$	$\bar{N}_G$	$\bar{T} / \text{s}$	$\bar{N}_{\text{EST}}$
MCS	4.2994	0.2067	-	$1 \times 10^6$	-	-
AK-MCS	4.2926	0.2076	0.211	38.55	86.73	$1.460 \times 10^7$
CFAK-MCS <sup>b</sup>	4.2970	0.2091	0.094	44.60	2.49	$1.980 \times 10^5$
CFAK-MCS <sup>p</sup>	4.2988	0.2063	0.032	38.00	2.16	$1.650 \times 10^5$
CFAK-MCS <sup>c</sup>	4.3010	0.2054	0.074	36.70	2.24	$1.585 \times 10^5$

**Table 5** Results of Example 2 for the case of  $k = 3.9$  (50 runs).

Method	$\mu_{\hat{P}_f} /10^{-5}$	$\sigma_{\hat{P}_f} /10^{-5}$	$\bar{\varepsilon}_{\hat{P}_f} /%$	$\bar{N}_G$	$\bar{T} /s$	$\bar{N}_{EST}$
MCS	5.7718	0.3114	-	$8 \times 10^6$	-	-
AK-MCS	5.7653	0.3168	0.226	42.03	6785.64	$5.004 \times 10^8$
CFAK-MCS <sup>b</sup>	5.7713	0.3123	0.095	40.32	17.45	$1.766 \times 10^5$
CFAK-MCS <sup>p</sup>	5.7688	0.3153	0.134	31.88	14.90	$1.344 \times 10^5$
CFAK-MCS <sup>c</sup>	5.7693	0.3093	0.139	30.64	14.80	$1.297 \times 10^5$

Under the setting of  $k = 3.9$ , the failure probability is reduced by an order of magnitude than that under the setting of  $k = 3.4$ , and the difficulty of reliability analysis is significantly increased. Due to the PSO's ability to more accurately locate representative sample points through optimization algorithms, CFAK-MCSs achieve extremely high surrogate model accuracy with an average error in failure probability of only 0.139%. As shown by **Table 5**, the number of DoE samples required for the CFAK-MCSs to construct the surrogate model is less than that of AK-MCS. To ensure the reliability of the estimated failure probability, AK-MCS requires a large number of candidate samples, resulting in a sharp increase in the number of performance function value predictions during surrogate model construction and a corresponding increase in CPU time. As indicated in **Table 5**, AK-MCS predicts approximately  $5.004 \times 10^8$  performance function values for candidate samples during surrogate model construction, resulting in CPU time of nearly 2 hours. In contrast, CFAK-MCS<sup>b</sup> require only  $1.77 \times 10^5$  performance function value predictions or fewer during surrogate model construction, resulting in CPU time that is about 1/400 of that of AK-MCS. Compared with CFAK-MCS<sup>b</sup>, the number of DoE samples required by CFAK-MCS<sup>p</sup> and CFAK-MCS<sup>c</sup> are significantly reduced, which indicates the impact of penalty intensity control. In addition, the performance improvement of CFAK-MCS<sup>b</sup> compared to CFAK-MCS<sup>p</sup> is relatively low in this example, because the restriction on dense for the DOE sample density is relatively relaxed at a distance from the sampling center according to the current density control method. It is worth mentioning that for small failure probability problems, a stricter restriction on dense of DoE samples at the limit state may seriously affect the solution accuracy of failure probability.

To be more intuitive, the predicted LSF and distribution of DoE samples obtained by CFAK-MCS<sup>b</sup> and CFAK-MCS<sup>c</sup> for one of the 50 runs are shown in **Fig. 15** and **Fig. 16**, respectively. In this run, both CFAK-MCS<sup>b</sup> and CFAK-MCS<sup>c</sup> achieve satisfactory solution accuracy of failure probability ( $\hat{P}_f = 5.3625 \times 10^{-5}$  and  $\varepsilon_{\hat{P}_f} = 0.00\%$ ) and the size of DoE required by them is 40 and 29, respectively. **Fig. 15** depicts the predicted LSF with 13 and 40 DoE samples, respectively, and

**Fig. 16**, depicts the predicted LSF with 6, 13, 18 and 29 DoE samples. It can be seen from **Fig. 15** and **Fig. 16** that CFAK-MCS<sup>b</sup> selects the representative sample points close to the LSF at the beginning of the surrogate model construction, while the representative sample points obtained by CFAK-MCS<sup>c</sup> at the beginning of surrogate model construction are gradually away from the sampling center, which reflects the impact of penalty intensive distribution control. The predicted LSF under various DoEs are represented by solid blue lines, while the real LSF is represented by the red lines. It can be observed that as the number of DoE samples increases, the predicted LSF of the surrogate model gradually converge towards the real LSF. Ultimately, failure points can be accurately incorporated into the predicted LSF to obtain an accurate failure probability.

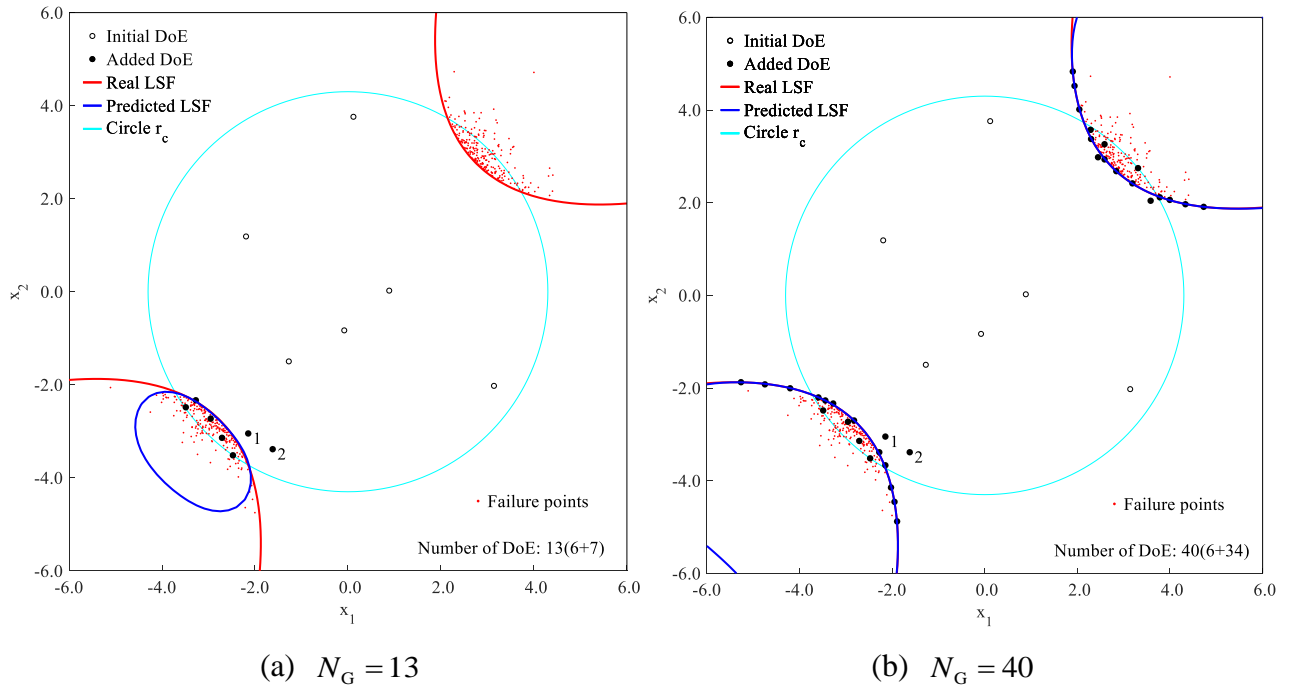
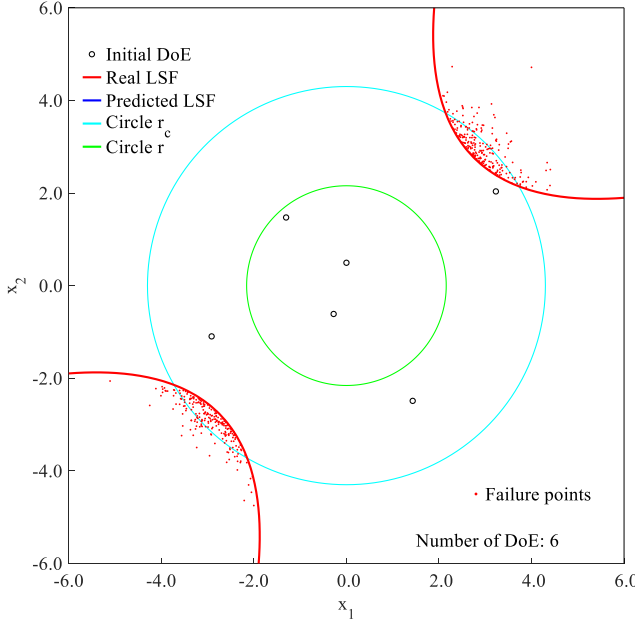
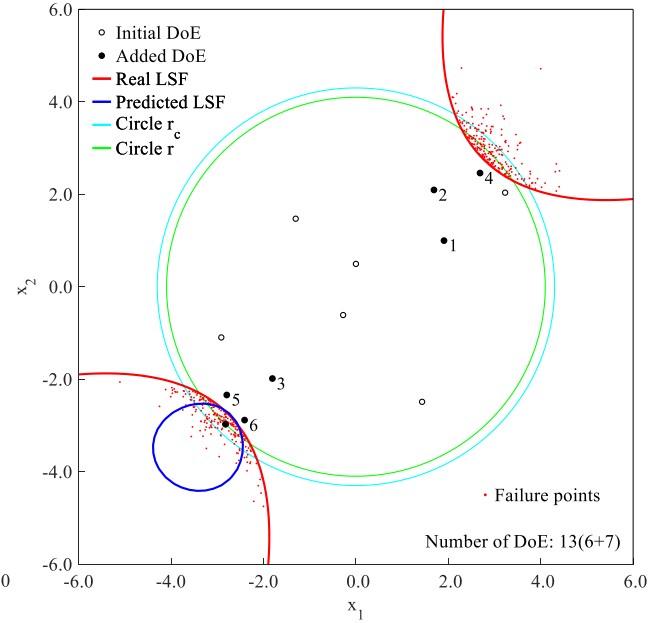


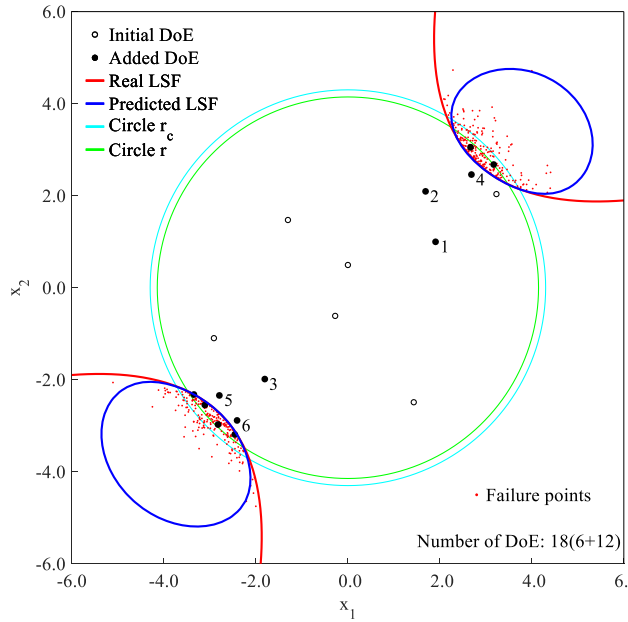
**Fig. 15.** The predicted LSF and DoE obtained by CFAK-MCS<sup>b</sup> ( $k = 3.9$ ).



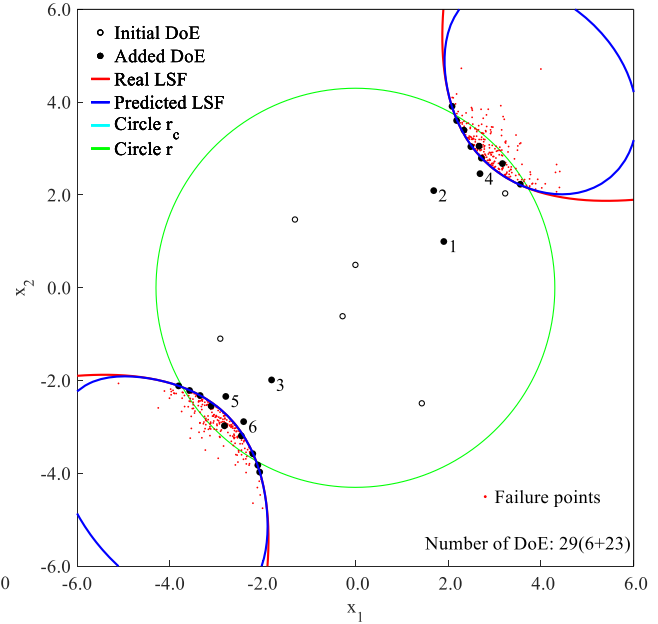
(a)  $N_{\text{DoE}} = 6$



(b)  $N_{\text{DoE}} = 13$



(c)  $N_{\text{DoE}} = 18$



(d)  $N_{\text{DoE}} = 29$

**Fig. 16.** The predicted LSF and DoE obtained by CFAK-MCS<sup>c</sup> ( $k = 3.9$ ).

Based on the research presented in this section, several key insights have been gained. Firstly, the selection of representative samples through an optimization algorithm is effective, and an adaptive surrogate model based on optimization can accurately approximate the real performance function. Secondly, the incorporation of penalty intensity control more accurately reflects the influence of sample position on the accuracy of failure probability estimation, thereby reducing the size of DoE samples required for surrogate model construction. Thirdly, the use of density control

prevents the selection of sample points that do not contribute significantly to the surrogate model, further reducing the size of DoE. Additionally, the intensity of density control varies with spatial position and can be relaxed in edge regions to improve solution accuracy for small failure probability problems. Given that both penalty intensity control and density control enhance the performance of the proposed CSP-free AK-MCS, CFAK-MCS<sup>c</sup> is employed as the proposed method in subsequent numerical examples (Examples 3-5).

#### 4.3. Example 3: The modified Rastrigin function

The modified version of the Rastrigin function, which is a highly nonlinear performance function involving non-convex and scattered gaps of failure domains, is taken in consideration. This problem is usually employed to test the validity of reliability methods [31, 33, 35] and the performance function is expressed as follows

$$G(\mathbf{x}) = 10 - \sum_{i=1}^2 (x_i^2 - 5\cos(2\pi x_i)) \quad (31)$$

where  $x_1$  and  $x_2$  are two independent standard normal distributed random variables. The failure probability of this problem is obtained by using CFAK-MCS<sup>c</sup> and compared with various other methods, among which the MCS result taken from [48] is used as the reference, and the results of AK-MCS+U/AK-MCS+EFF [14], REAK [48], MetaAK-IS2 [49] and AKSE/AKSE-b [35] taken from the corresponding references are also listed for comparison purpose. In CFAK-MCS<sup>c</sup>, the number of samples for the initial DoE is set to 20 and the control parameters for PSO are set to  $N_{\text{swarm}} = 100$ ,  $N_{\text{ite\_max}} = 50$ ,  $V_{\text{max}} = 0.3$ ,  $\omega = 0.729$  and  $c_1 = c_2 = 2.0$ . In the second stage of CFAK-MCS<sup>c</sup>,  $6 \times 10^4$  samples used in MCS are evaluated to estimate the failure probability. For a performance function that is highly nonlinear and has non-convex and scattered failure domains, it is necessary to relax the distance constraint on the DoE to more accurately describe the failure regions. As such, the parameter used to describe the distance constraint is set to  $r_d = 0.1$ . To avoid difficulties in terminating surrogate model construction due to repeated acquisition of points precisely located on the LSF,  $\delta$  in Eq. (23) is set to 0.1. This allows for the identification of representative sample points within the failure regions rather than on the LSF. Different settings of  $r_c$  are considered for CFAK-MCS<sup>c</sup> and the results obtained by different methods are summarized in

**Table 6.** Meanwhile, **Fig. 17** shows the predicted LSF, DoE, and estimated failure probability results of one run under different settings of  $r_c$ .

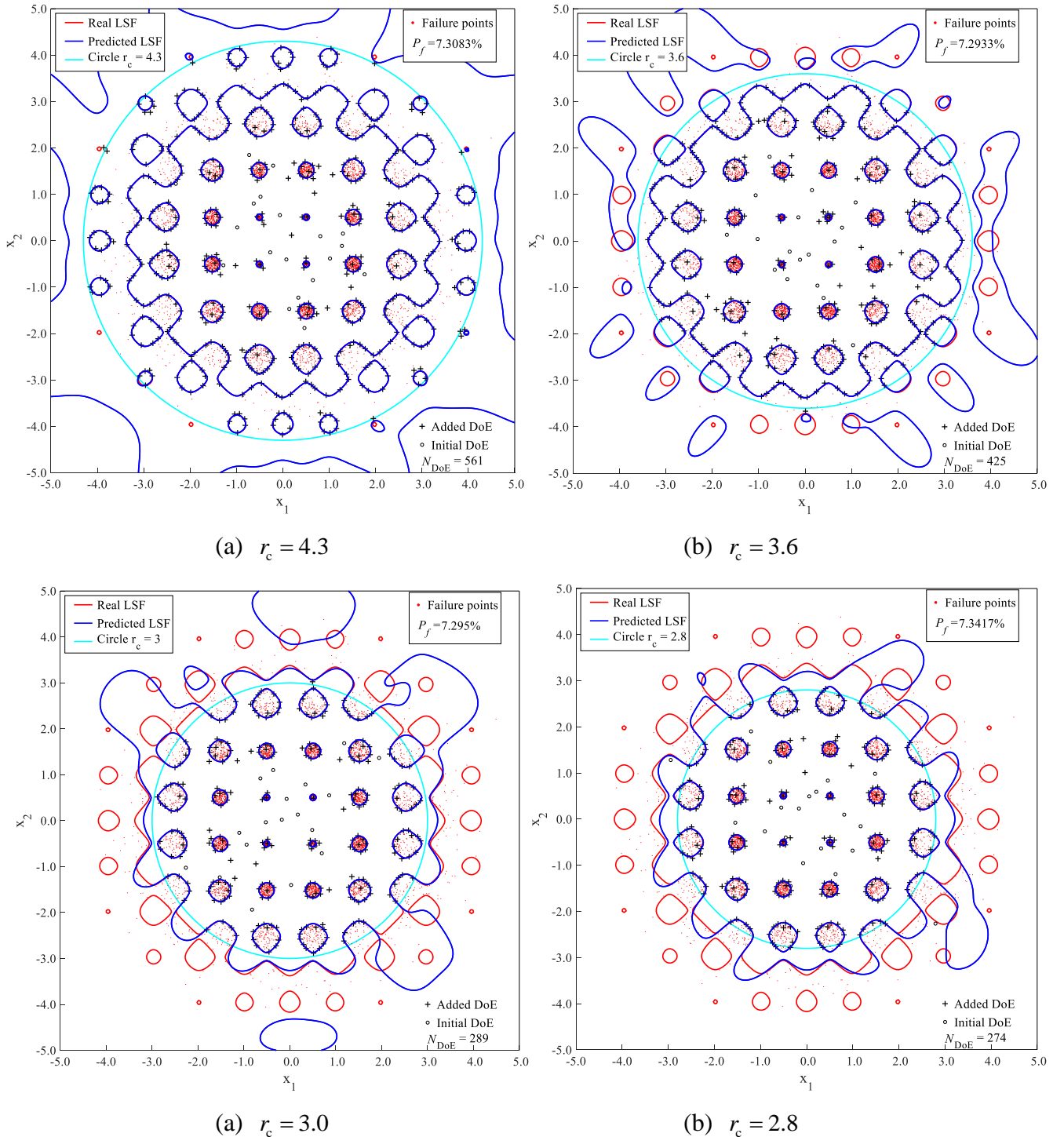


**Fig. 17.** The predicted LSF and DoE for Example 3.

**Table 6** Reliability analysis results of Example 3 using different methods.

Method	$r_c$	$\hat{P}_f /10^{-2}$	$\hat{\beta}$	$N_G$	$\varepsilon_{\hat{P}_f} /%$	$V_{\hat{P}_f} /%$	CPU time/s
MCS	-	7.308	1.453	$6 \times 10^4$	-	1.45	-
AK-MCS+U	-	7.340	1.451	416	0.44	1.45	-
AK-MCS+EFF	-	7.340	1.451	417	0.44	1.45	-
REAK	-	7.277	1.456	401	0.42	<1.50	-
MetaAK-IS <sup>2</sup>	-	7.350	1.450	480	0.57	2.50	-
AKSE	-	7.254	1.457	263.5	0.74	1.13	805.4
AKSE-b	-	7.229	1.459	258.1	1.08	1.13	27593.8
CFAK-MCS <sup>c</sup>	4.3	7.308	1.453	556.0	0.00	1.45	146.6
	3.6	7.294	1.454	415.5	0.20	1.46	65.0
	3.0	7.312	1.453	297.1	0.05	1.45	28.1
	2.9	7.299	1.454	286.5	0.13	1.45	25.8
	2.8	7.275	1.456	266.6	0.45	1.46	20.6
	2.7	7.140	1.466	243.8	2.30	1.47	16.9

Note:  $\hat{\beta}$  is the probability index

As shown in **Table 6**, the setting of  $r_c$  has an impact on the computational performance of CFAK-MCS<sup>c</sup>. For this example, with the increase of  $r_c$ , more DoE samples are required to complete the construction of a surrogate model, and the precision of the established surrogate model is correspondingly improved. For instance, when  $r_c$  is set to 4.3, the construction of a surrogate model requires approximately 556 DOE samples, and the estimated failure probability is almost consistent with the reference (with a relative error of less than 0.01%). Correspondingly, as shown in **Fig. 17a**, the predicted LSF obtained under the setting of  $r_c = 4.3$  is almost identical to the real LSF. With the decrease of  $r_c$ , the number of DoE samples required to complete the construction of a surrogate model gradually decreases. When the parameter  $r_c$  is set to 3.0, the number of DoE samples required to build the surrogate model is approximately 297, which is less than most other methods. As shown in **Fig. 17**, with the decrease in  $r_c$ , there are some differences between the predicted LSF and the real LSF in the regions outside the circular area with radius  $r_c$ . This affects, to some extent, the accuracy of the predicted failure probability obtained by CFAK-MCS<sup>c</sup>. However, as shown in **Table 6**, CFAK-MCS<sup>c</sup> can still achieve high computational accuracy at  $r_c \in [2.8, 4.3]$  compared to other methods listed. The author believes that in this example, ensuring the accuracy of estimated failure probability lies in accurately describing the LSF in the area closer to the sampling

center. In other words, even if the LSF cannot be accurately described at the sampling edge, its impact on the accuracy of failure probability estimation is relatively insignificant. It should also be noted that the value of  $r_c$  should not be set too low; otherwise, it will lead to a deviation in predicted LSF within large regions and affect failure probability accuracy. For example, under the setting of  $r_c = 2.7$ , the relative error of failure probability reaches 2.3%. Since the proposed method does not require failure probability estimation during surrogate model construction, repeated prediction of sampling populations can be avoided. In fact, sample prediction required in PSO process is far less than that for the CSP. Therefore, workload for this example is relatively low. As shown in **Table 6**, under the settings of  $r_c = 4.3$  and  $r_c = 3.0$ , the CPU time is only about 147 s and 28 s, respectively, reflecting the efficiency advantage of the proposed method.

#### 4.4. Example 4: A highly nonlinear problem

A 2D analytical example previously studied in [16, 50, 51] is chosen to test the performance of CFAK-MCS<sup>c</sup> on a high nonlinearity problem with a single failure region. The performance function is given as:

$$G(\mathbf{x}) = 1.2 - \frac{1}{20} (x_1^2 + 4)(x_2 - 1) + \sin\left(\frac{5}{2}x_1\right) \quad (32)$$

where  $x_1$  and  $x_2$  are two independent standard normal variables. The results of the proposed CFAK-MCS<sup>c</sup> are compared with those obtained by MCS, FORM, SORM, REIF [16], AK-MCS+U/AK-MCS+EFF [14], ESC+U [52] and AKSE/AKSE-b [35]. The estimated failure probability obtained by MCS with  $1 \times 10^6$  samples is used as the reference. In CFAK-MCS<sup>c</sup>, the number of samples for the initial DoE is set to 8 and the control parameters for PSO are the same as those in Example 3. For the second stage of CFAK-MCS<sup>c</sup>,  $1 \times 10^6$  samples used in MCS are evaluated to estimate the failure probability. Different settings of  $r_c$  are considered for CFAK-MCS<sup>c</sup> and all of the results obtained by different methods are summarized in **Table 7**. Meanwhile, **Fig. 18** shows the predicted LSF, DoE, and estimated failure probabilities of one run under different settings of  $r_c$ .

As indicated in **Table 7**, the failure probabilities estimated by FORM and SORM are inaccurate with relatively large errors, despite requiring far more functional calls than the surrogate-based methods. CFAK-MCS<sup>c</sup> achieves acceptable results for this example. Similar to Example 3, when  $r_c$  is set to a higher value (such as  $r_c = 4.3$ ), the solution accuracy is high and the number of DoE samples is large, as reflected in **Fig. 18a**). As the parameter  $r_c$  decreases, the number of DoE samples and the solution accuracy correspondingly decrease. Under the setting of

$r_c = 3.6$ , the number of DoE samples required to construct the surrogate model is equivalent to that of AK-MCS. Under the setting of  $r_c = 3.2$ , CFAK-MCS<sup>c</sup> can achieve an optimal balance between solution accuracy and efficiency. At this setting, the number of DoE samples is smaller than that of AK-MCS, and the relative error of estimated failure probability is less than 1.0%. In term of CPU time, CFAK-MCS<sup>c</sup> demonstrates an extremely high advantage. Compared with AK-MCS, the CPU time of CFAK-MCS<sup>c</sup> is less than 1/6 of the former when the number of DOE samples required by the two methods is similar.

**Table 7** Reliability analysis results of Example 4 using different methods.

Method	$r_c$	$\hat{P}_f / 10^{-3}$	$\hat{\beta}$	$N_G$	$\varepsilon_{\hat{P}_f} / \%$	$V_{\hat{P}_f} / \%$	CPU time/s
MCS	-	4.710	2.596	$1 \times 10^6$	-	1.45	-
FORM	-	2.563	1.949	779	45.58	-	-
SORM	-	3.671	2.681	791	22.06	-	-
REIF	-	4.720	2.586	42.3	0.23	0.52	-
AK-MCS+U	-	4.711	2.596	58.9	0.02	2.06	30.5
AK-MCS+EFF	-	4.716	2.696	57.1	0.13	2.05	29.3
ESC+U	-	4.708	2.597	45.3	0.04	2.06	89.6
AKSE	-	4.714	2.596	30.7	0.08	2.05	170.3
AKSE-b	-	4.703	2.597	30.4	0.15	2.06	3500.4
CFAK-MCS <sup>c</sup>	4.3	4.709	2.596	82.0	0.01	1.45	6.99
	3.6	4.695	2.598	58.2	0.32	1.46	4.31
	3.2	4.683	2.598	51.4	0.56	1.46	3.73
	3.1	4.652	2.601	46.7	1.23	1.46	3.33

Note: the results of other methods are obtained from [35],  $\hat{\beta}$  is the probability index.

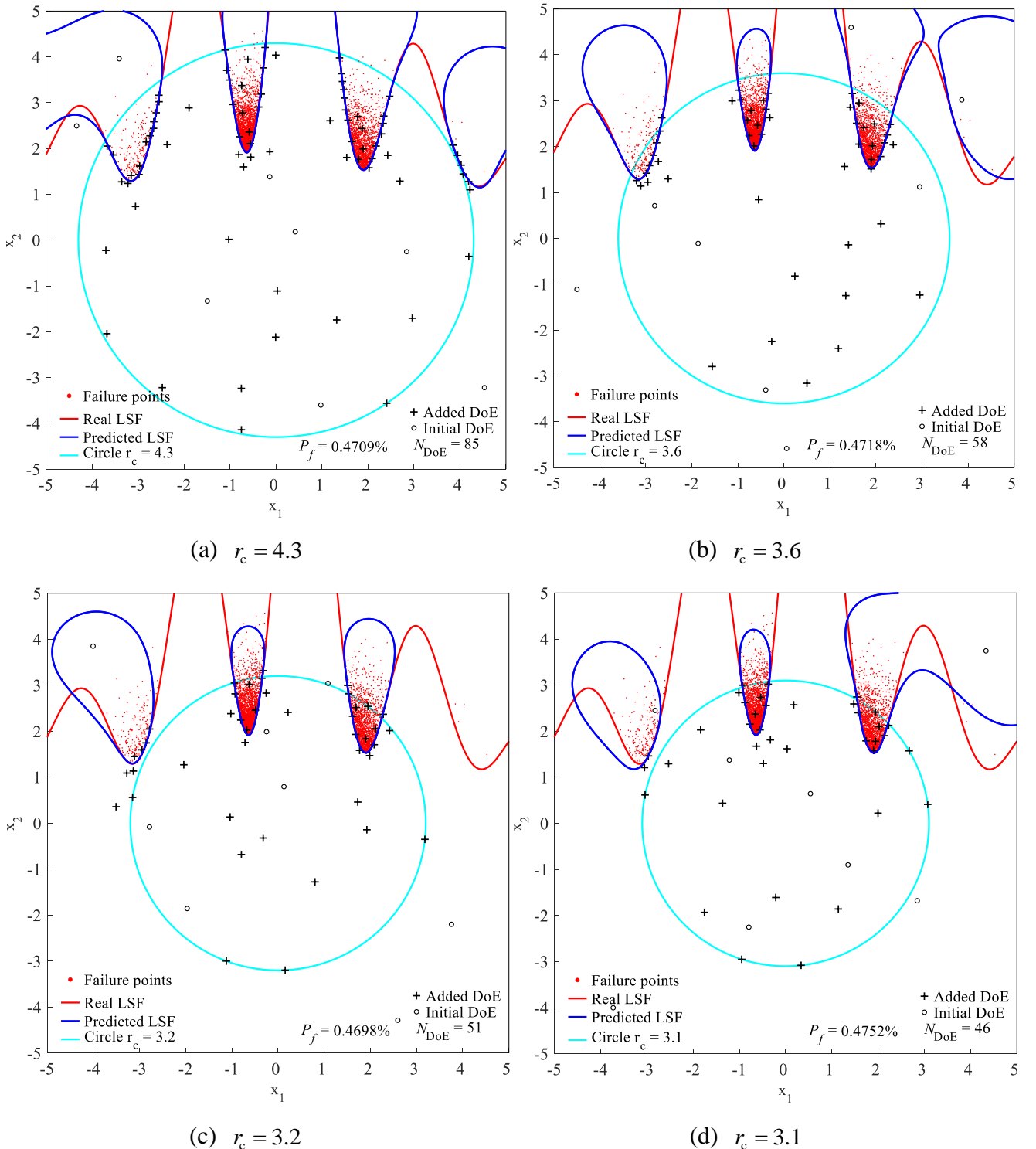


**Fig. 18.** The predicted LSF and DoE for Example 4.

#### 4.5. Example 5: Dynamic response of a nonlinear oscillator

The reliability analysis of an undamped single degree of freedom system-a nonlinear oscillator subjected to a rectangular load pulse (as shown in **Fig. 19**) is conducted. The performance function of this nonlinear dynamic system is given as

$$G(c_1, c_2, m, r, t_1, F_1) = 3r - \left| \frac{2F_1}{m\omega_0^2} \sin\left(\frac{\omega_0 t_1}{2}\right) \right| \quad (33)$$

where

$$\omega_0 = \sqrt{(c_1 + c_2)/m} \quad (34)$$

Two cases with different distribution parameters of  $F_1$  are analyzed to investigate the effectiveness of the proposed method for problems. The distribution parameters of these random variables are listed in **Table 8**.

The results of the proposed CFAK-MCS<sup>c</sup> are compared with those obtained by other methods. In CFAK-MCS<sup>c</sup>, the number of samples for the initial DoE is set to 13 and the control parameters for PSO are the same as those in Example 3. If no otherwise specified, the samples used in MCS are evaluated to estimate the failure probability in the second stage of CFAK-MCS<sup>c</sup>.

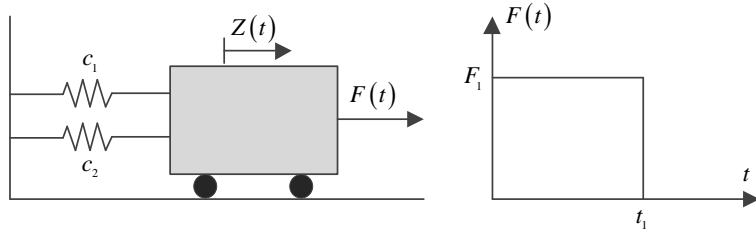


**Fig. 19.** Nonlinear oscillator subjected to a rectangular load pulse.

For Case 1, the results of the proposed CFAK-MCS<sup>c</sup> are compared with those obtained by MCS, AK-SS [53], AK-MSS [31], AWL-MSS [38], AK-MCS+U/AK-MCS+EFF [14], ESC+U [52], AKSE/AKSE-b [35]. Different settings of  $r_c$  are considered for CFAK-MCS<sup>c</sup> and all of the results obtained by different methods are summarized in **Table 9**. The estimated failure probability obtained by MCS with  $1 \times 10^6$  samples is used as the reference. **Table 9** shows that highly accurate estimated failure probability ( $\varepsilon_{\hat{P}_f} < 0.1\%$ ) can be obtained under the setting of  $r_c \in [2.1, 4.3]$ , demonstrating the advantage of CFAK-MCS<sup>c</sup> compared to most listed methods. Similar to Example 3 and Example 4, the number of DOE samples decreases with the decrease of  $r_c$ . For Case 1, with a high failure probability of 2.859%, only 36.8 DOE samples are required under the setting of  $r_c = 2.1$ . This is less than the other methods listed in **Table 9**. At this setting, the relative error of estimated failure probability is only 0.07%, indicating relatively high solution accuracy. These results demonstrate that the method proposed in this paper can also exhibit extremely high computational performance in cases with multiple random variables. In terms of CPU time,

CFAK-MCS<sup>c</sup> takes less than 6 seconds to complete a failure probability estimation, significantly less than other methods listed in the table.

**Table 8** Statistical information of the random variables for Example 5.

Random variable	Distribution	Mean	Standard deviation
$m$	Normal	1	0.05
$c_1$	Normal	1	0.1
$c_2$	Normal	0.1	0.01
$r$	Normal	0.5	0.05
$t_1$	Normal	1	0.2
$F_1$ (Case 1)	Normal	1	0.2
$F_1$ (Case 2)	Normal	0.6	0.1

**Table 9** Reliability analysis results of Example 5 (Case 1) using different methods.

Method	$r_c$	$\hat{P}_f /10^{-2}$	$\hat{\beta}$	$N_G$	$\varepsilon_{\hat{P}_f} /%$	$V_{\hat{P}_f} /%$	CPU time/s
MCS	-	2.859	1.902	$1 \times 10^6$	-	0.58	-
AK-SS	-	2.833	1.906	410	0.91	-	-
AK-MSS	-	2.870	1.900	86	0.38	-	-
AWL-MCS	-	2.826	1.907	65	1.15	-	-
AK-MCS-U	-	2.850	1.903	147.2	0.31	1.85	108.4
AK-MCS+EFF	-	2.867	1.901	126.8	0.28	1.84	86.7
ESC+U	-	2.866	1.901	56.2	0.24	1.84	42.1
AKSE	-	2.862	1.902	38.6	0.10	1.84	36.4
AKSE-b	-	2.851	1.903	42.0	0.28	1.85	1371.7
CFAK-MCS <sup>c</sup>	4.3	2.860	1.902	74.2	0.03	0.58	5.98
	3.6	2.861	1.902	64.9	0.04	0.58	5.06
	3.1	2.861	1.902	57.1	0.08	0.58	4.37
	2.6	2.861	1.902	46.3	0.05	0.58	3.55
	2.1	2.857	1.902	36.8	0.07	0.58	2.97
	1.6	2.863	1.901	37.9	0.14	0.58	3.03

Note: the results of other methods are obtained from [35],  $\hat{\beta}$  is the probability index.

For Case 2, the results of the proposed CFAK-MCS<sup>c</sup> are compared with those obtained by MCS, AK-IS+U/AK-IS+EFF, ESC-IS+U and AKSE/AKSE-b, and the results obtained by different methods are summarized in **Table 10**, where the estimated failure probability obtained by MCS is

used as the reference. It should be noted that Case 2 is a small failure probability problem ( $\hat{P}_f = 9.090 \times 10^{-6}$ ), and hence a large size of Monte Carlo population ( $1.8 \times 10^8$ ) is set to ensure the reliability of MCS results. For the second stage of CFAK-MCS<sup>c</sup>, two implementations are considered: one estimates failure probability based on a Monte Carlo population with  $1.8 \times 10^8$  samples, and the second estimates failure probability by adding  $1.0 \times 10^7$  samples step by step according to **Sec. 3.2.1**. To distinguish between these implementations, the subscript ‘\*’ is used to indicate the latter implementation. As shown by **Table 10**, the proposed method completes surrogate model construction with a small number of DOE samples and achieves high solution accuracy. In the ‘CPU time’ column, results corresponding to CFAK-MCS<sup>c</sup> are expressed as ‘ $T_1+T_2$ ’, where  $T_1$  and  $T_2$  represent CPU time for surrogate model construction and failure probability estimation using the established surrogate model, respectively. As shown in **Table 10**, it only takes 3.3 seconds to complete the construction of a surrogate model in CFAK-MCS<sup>c</sup>. In other words, most CPU time is spent on predicting all samples using the established surrogate model. For example, it takes approximately 500 seconds to complete prediction of  $1.8 \times 10^8$  samples. It should be noted that the second stage of CFAK-MCS<sup>c</sup> does not change the accuracy of a surrogate model but only provides a numerical representation of its accuracy. In fact, several methods can reduce time consumption in the second stage, such as using importance sampling and parallel computing. For instance, CFAK-MCS<sup>c\*</sup> listed in **Table 10** has a sample size of  $6 \times 10^7$  in the second stage; not only are solution accuracy and DOE size satisfactory, but its total CPU time is also quite small.

**Table 10** Reliability analysis results of Example 5 (Case 2) using different methods.

Method	$r_c$	$\hat{P}_f / 10^{-6}$	$\hat{\beta}$	$N_G$	$\varepsilon_{\hat{P}_f} / \%$	$V_{\hat{P}_f} / \%$	CPU time/s
MCS	-	9.090	4.286	$1.8 \times 10^8$	-	2.47	-
AK-IS+U	-	9.108	4.286	281.6	0.20	2.94	3036.9
AK-IS+EFF	-	9.161	4.284	182.3	0.78	2.59	1301.1
ESC-IS+U	-	9.178	4.284	54.1	0.97	3.10	267.9
AKSE-IS	-	9.032	4.288	47.2	0.64	1.91	269.7
AKSE-b-IS	-	9.130	4.285	49.3	0.44	2.92	6466.3
CFAK-MCS <sup>c</sup>	4.3	9.114	4.286	41.4	0.26	2.47	3.3+507.2
	3.0	9.063	4.287	42.8	0.30	2.48	3.3+516.1
CFAK-MCS <sup>c*</sup>	4.3	9.061	4.286	41.2	0.32	4.28	3.3+173.8
	3.0	9.054	4.287	42.3	0.40	4.29	3.3+176.2

Note: the results of other methods are obtained from [35],  $\hat{\beta}$  is the probability index.

## 5. Conclusions

This study proposes a CSP-free adaptive Kriging surrogate model method for reliability analysis with small failure probabilities. The surrogate model is iteratively refined, and representative samples are chosen for updating the surrogate model through an optimization solution facilitated by the particle swarm optimization algorithm. To achieve an optimal balance between solution accuracy and efficiency, penalty intensity control and density control for the experimental design points are introduced to modify the objective function in optimization. Numerical examples are used to validate the proposed method and evaluate its computational performance. The following conclusions can be drawn:

- (1) The incorporation of a particle swarm optimization algorithm effectively increases the likelihood of obtaining representative samples for constructing the surrogate model, resulting in an improvement in solution accuracy for an adaptive Kriging surrogate model method in reliability analysis.
- (2) The proposed CSP-free surrogate model method separates surrogate model construction and failure probability evaluation into two distinct stages, resulting in a more transparent implementation process. Firstly, there is no need to repeatedly evaluate the variation coefficient of failure probability during surrogate model construction. In addition, the method has ability to capture representative sample points in sparse distribution regions. Therefore, the proposed method is suitable for reliability analysis with small failure probability.
- (3) The introduction of penalty intensity control and density control for the objective function plays an important role in reasonable selection of representative samples for updating the surrogate model, thereby improving the performance of the adaptive surrogate model method.

Although only basic numerical examples are used, they are sufficient to demonstrate the effectiveness of the proposed methodology. For problems involving random variables with different distribution characteristics, Monte Carlo sampling can still be performed using the standard normal distribution, with a specific transformation applied to account for the influence of the actual distribution before calculating the performance function. For the reliability assessment of real engineering structures with multiple failure modes, the failure probability can be determined through Monte Carlo sampling using the adaptive surrogate model, as long as the effects of different failure modes are appropriately incorporated into the performance function. As a result, the proposed adaptive surrogate model methodology can be easily extended to address challenges such as various types of random variables and multiple failure modes, providing robust solutions for

practical applications.

## Acknowledgments

The project is funded by the National Natural Science Foundation of China (Grant No. 52178209, Grant No. 51878299) and Guangdong Basic and Applied Basic Research Foundation, China (Grant No. 2020A1515010611, Grant No. 2021A1515012280).

## References

- [1] S.K. Au, J.L. Beck. A new adaptive importance sampling scheme for reliability calculations. *Structural Safety* 1999; 21: 135-58.
- [2] W. Zhao, F. Fan, W. Wang. Non-linear partial least squares response surface method for structural reliability analysis. *Reliability Engineering & System Safety* 2017; 161: 69-77.
- [3] X. Tan, W. Bi, X. Hou, W. Wang. Reliability analysis using radial basis function networks and support vector machines. *Computers and Geotechnics* 2011; 38: 178-86.
- [4] P. Yi, K. Wei, X. Kong, Z. Zhu. Cumulative PSO-Kriging model for slope reliability analysis. *Probabilistic Engineering Mechanics* 2015; 39: 39-45.
- [5] A.A. Chojczyk, A.P. Teixeira, L.C. Neves, J.B. Cardoso, et al. Review and application of Artificial Neural Networks models in reliability analysis of steel structures. *Structural Safety* 2015; 52: 78-89.
- [6] J. Feng, L. Liu, D. Wu, G. Li, et al. Dynamic reliability analysis using the extended support vector regression (X-SVR). *Mechanical Systems and Signal Processing* 2019; 126: 368-91.
- [7] J.M. Bourinet, F. Deheeger, M. Lemaire. Assessing small failure probabilities by combined subset simulation and Support Vector Machines. *Structural Safety* 2011; 33: 343-53.
- [8] Q. Pan, D. Dias. An efficient reliability method combining adaptive Support Vector Machine and Monte Carlo Simulation. *Structural Safety* 2017; 67: 85-95.
- [9] X. Li, C. Gong, L. Gu, W. Gao, et al. A sequential surrogate method for reliability analysis based on radial basis function. *Structural Safety* 2018; 73: 42-53.
- [10] N. Xiao, M.J. Zuo, C. Zhou. A new adaptive sequential sampling method to construct surrogate models for efficient reliability analysis. *Reliability Engineering & System Safety* 2018; 169: 330-38.
- [11] V. Papadopoulos, D.G. Giovanis, N.D. Lagaros, M. Papadrakakis. Accelerated subset simulation with neural networks for reliability analysis. *Computer Methods in Applied Mechanics and Engineering* 2012; 223-224: 70-80.
- [12] Y. Ma, M. Liu, H. Nan, H. Li, et al. A novel hybrid adaptive scheme for Kriging-based reliability estimation – A comparative study. *Applied Mathematical Modelling* 2022; 108: 1-26.
- [13] N. Xiao, M.J. Zuo, W. Guo. Efficient reliability analysis based on adaptive sequential sampling design and cross-validation. *Applied Mathematical Modelling* 2018; 58: 404-20.

[14] B. Echard, N. Gayton, M. Lemaire. AK-MCS: An active learning reliability method combining Kriging and Monte Carlo Simulation. *Structural Safety* 2011; 33: 145-54.

[15] W. Fauriat, N. Gayton. AK-SYS: An adaptation of the AK-MCS method for system reliability. *Reliability Engineering & System Safety* 2014; 123: 137-44.

[16] X. Zhang, L. Wang, J.D. Sørensen. REIF: A novel active-learning function toward adaptive Kriging surrogate models for structural reliability analysis. *Reliability Engineering & System Safety* 2019; 185: 440-54.

[17] W. Yun, Z. Lu, Y. Zhou, X. Jiang. AK-SYSi: an improved adaptive Kriging model for system reliability analysis with multiple failure modes by a refined U learning function. *Structural and Multidisciplinary Optimization* 2019; 59: 263-78.

[18] N. Xiao, K. Yuan, C. Zhou. Adaptive kriging-based efficient reliability method for structural systems with multiple failure modes and mixed variables. *Computer Methods in Applied Mechanics and Engineering* 2020; 359: 112649.

[19] J. Wang, Z. Sun, R. Cao. An efficient and robust Kriging-based method for system reliability analysis. *Reliability Engineering & System Safety* 2021; 216: 107953.

[20] Y. Xiong, S. Sampath. A fast-convergence algorithm for reliability analysis based on the AK-MCS. *Reliability Engineering & System Safety* 2021; 213: 107693.

[21] N. Xiao, K. Yuan, H. Zhan. System reliability analysis based on dependent Kriging predictions and parallel learning strategy. *Reliability Engineering & System Safety* 2022; 218: 108083.

[22] Y. Ma, Y. Zhu, H. Li, H. Nan, et al. Adaptive Kriging-based failure probability estimation for multiple responses. *Reliability Engineering & System Safety* 2022; 228: 108771.

[23] B. Echard, N. Gayton, M. Lemaire, N. Relun. A combined Importance Sampling and Kriging reliability method for small failure probabilities with time-demanding numerical models. *Reliability Engineering & System Safety* 2013; 111: 232-40.

[24] M. Balesdent, J. Morio, J. Marzat. Kriging-based adaptive Importance Sampling algorithms for rare event estimation. *Structural Safety* 2013; 44: 1-10.

[25] H. Zhao, Z. Yue, Y. Liu, Z. Gao, et al. An efficient reliability method combining adaptive importance sampling and Kriging metamodel. *Applied Mathematical Modelling* 2015; 39: 1853-66.

[26] W. Yun, Z. Lu, X. Jiang. An efficient reliability analysis method combining adaptive Kriging and modified importance sampling for small failure probability. *Structural and Multidisciplinary Optimization* 2018; 58: 1383-93.

[27] Z. Sun, J. Wang, R. Li, C. Tong. LIF: A new Kriging based learning function and its application to structural reliability analysis. *Reliability Engineering & System Safety* 2017; 157: 152-65.

[28] N. Lelièvre, P. Beaurepaire, C. Matstrand, N. Gayton. AK-MCSi: A Kriging-based method to deal with small failure probabilities and time-consuming models. *Structural Safety* 2018; 73: 1-11.

[29] Z. Lv, Z. Lu, P. Wang. A new learning function for Kriging and its applications to solve reliability

problems in engineering. *Computers & Mathematics with Applications* 2015; 70: 1182-97.

- [30] C. Zhou, N. Xiao, X. Li, J. Zhang. Structural reliability analysis using circular sampling surrogate models. *Journal of University of Electronic Science and Technology of China*. 2021; 50: 155-60 (in Chinese).
- [31] C. Xu, W. Chen, J. Ma, Y. Shi, et al. AK-MSS: An adaptation of the AK-MCS method for small failure probabilities. *Structural Safety* 2020; 86: 101971.
- [32] W. Yun, Z. Lu, X. Jiang, L. Zhang, et al. AK-ARBIS: An improved AK-MCS based on the adaptive radial-based importance sampling for small failure probability. *Structural Safety* 2020; 82: 101891.
- [33] Z. Liu, Z. Lu, C. Ling, K. Feng, et al. An improved AK-MCS for reliability analysis by an efficient and simple reduction strategy of candidate sample pool. *Structures* 2022; 35: 373-87.
- [34] K. Song, Y. Zhang, L. Shen, Q. Zhao, et al. A failure boundary exploration and exploitation framework combining adaptive Kriging model and sample space partitioning strategy for efficient reliability analysis. *Reliability Engineering & System Safety* 2021; 216: 108009.
- [35] J. Wang, G. Xu, Y. Li, A. Kareem. AKSE: A novel adaptive Kriging method combining sampling region scheme and error-based stopping criterion for structural reliability analysis. *Reliability Engineering & System Safety* 2022; 219: 108214.
- [36] B.J. Bichon, M.S. Eldred, L.P. Swiler, S. Mahadevan, et al. Efficient global reliability analysis for nonlinear implicit performance functions. *AIAA Journal* 2008; 46: 2459-68.
- [37] Z. Jing, J. Chen, X. Li. RBF-GA: An adaptive radial basis function metamodeling with genetic algorithm for structural reliability analysis. *Reliability Engineering & System Safety* 2019; 189: 42-57.
- [38] Z. Meng, Z. Zhang, G. Li, D. Zhang. An active weight learning method for efficient reliability assessment with small failure probability. *Structural and Multidisciplinary Optimization* 2020; 61: 1157-70.
- [39] D. Wang, D. Tan, L. Liu. Particle swarm optimization algorithm: an overview. *Soft Computing* 2018; 22: 387-408.
- [40] Y. Gong, J. Li, Y. Zhou, Y. Li, et al. Genetic Learning Particle Swarm Optimization. *Ieee Transactions On Cybernetics* 2016; 46: 2277-90.
- [41] R. Eberhart, J. Kennedy. A new optimizer using particles swarm theory. In: *Proceedings of the Sixth international symposium on micro machine and human science*, Nagoya. 1995.
- [42] R.E. Perez, K. Behdinan. Particle swarm approach for structural design optimization. *Computers & Structures* 2007; 85: 1579-88.
- [43] G. Luh, C. Lin, Y. Lin. A binary particle swarm optimization for continuum structural topology optimization. *Applied Soft Computing* 2011; 11: 2833-44.
- [44] C. Elegbede. Structural reliability assessment based on particles swarm optimization. *Structural Safety* 2005; 27: 171-86.

[45] B. Bai, C. Zhou, N. Ye. Application of multi-failure mode reliability-based particle swarm optimization algorithm. *Computers & Industrial Engineering* 2021; 161: 107627.

[46] M. Clerc, J. Kennedy. The particle swarm - explosion, stability, and convergence in a multidimensional complex space. *Ieee Transactions On Evolutionary Computation* 2002; 6: 58-73.

[47] L. Schueremans, D. Van Gemert. Benefit of splines and neural networks in simulation based structural reliability analysis. *Structural Safety* 2005; 27: 246-61.

[48] Z. Wang, A. Shafeezadeh. REAK: Reliability analysis through Error rate-based Adaptive Kriging. *Reliability Engineering & System Safety* 2019; 182: 33-45.

[49] F. Cadini, F. Santos, E. Zio. An improved adaptive kriging-based importance technique for sampling multiple failure regions of low probability. *Reliability Engineering & System Safety* 2014; 131: 109-17.

[50] B.J. Bichon, M.S. Eldred, L.P. Swiler, S. Mahadevan, et al. Efficient Global Reliability Analysis for Nonlinear Implicit Performance Functions. *AIAA Journal* 2008; 46: 2459-68.

[51] J. Yi, Q. Zhou, Y. Cheng, J. Liu. Efficient adaptive Kriging-based reliability analysis combining new learning function and error-based stopping criterion. *Structural and Multidisciplinary Optimization* 2020; 62: 2517-36.

[52] Z. Wang, A. Shafeezadeh. ESC: an efficient error-based stopping criterion for kriging-based reliability analysis methods. *Structural and Multidisciplinary Optimization* 2019; 59: 1621-37.

[53] X. Huang, J. Chen, H. Zhu. Assessing small failure probabilities by AK-SS: An active learning method combining Kriging and Subset Simulation. *Structural Safety* 2016; 59: 86-95.